



HORIZON 2020



# Product Traceability and Uncertainty for the Ozone Profile Differential Absorption Lidar Product

**Version 0.1.10**

*GAIA-CLIM  
Gap Analysis for Integrated  
Atmospheric ECV Climate Monitoring  
Mar 2015 - Feb 2018*

**A Horizon 2020 project; Grant agreement: 640276**

**Date: 20 January 2018**

**Dissemination level: Final**

*Work Package 2; Compiled by  
Arnoud Apituley, Anne van Gijzel (KNMI)*



Royal Netherlands  
Meteorological Institute  
Ministry of Infrastructure  
and Water Management

## Table of Contents

1	Version history .....	3
2	Product overview .....	4
2.1	Guidance notes .....	5
3	Introduction.....	9
4	Instrument description.....	10
5	Product Traceability Chain .....	15
6	Element contributions .....	17
6.1	Emission sub-system (1) .....	17
6.2	Receiving sub-system (2).....	18
6.3	Receiver optical parameters (2a).....	19
6.4	Alignment (2b).....	20
6.5	Pre-processing (3) .....	22
6.5.1	Detection noise (3a) .....	22
6.5.2	Saturation (pulse pile-up) correction (3b).....	23
6.5.3	Background noise extraction (3c) .....	24
6.6	External inputs (4).....	27
6.6.1	Ozone absorption cross section differential (4a).....	27
6.6.2	Rayleigh extinction cross section differential (4b) .....	29
6.6.3	Interfering gases' cross section differential (4c).....	30
6.6.4	Oxygen absorption cross section differential (4d) .....	32
6.6.5	Interfering gases' atmospheric profiles (4e) .....	33
6.6.6	Uncertainty owing to air number density, temperature and pressure profiles (4f) ....	34
6.7	Spatiotemporal integration (5) .....	38
6.7.1	Propagation of uncertainty when combining two intensity ranges (5a).....	38
7	Uncertainty summary .....	40
8	Traceability uncertainty analysis .....	46
8.1	Recommendations .....	47
9	Conclusion .....	50
	References.....	51

## 1 Version history

Version	Principal updates	Owner	Date
0.1 draft	First draft	KNMI	12.12.2017
0.1.10	Final draft	KNMI	20.01.2018

## 2 Product overview

Product name: Ozone concentration profile

Product technique: Differential Absorption Lidar

Product measurand: Ozone (O<sub>3</sub>)

Product form/range: profile (ground to 50 km, 1-2 hours averaged)

Product dataset: Ozone concentration profile

Site/Sites/Network location:

- Table Mountain, Wrightwood CA, USA (Tropospheric)
- Mauna Loa, Hawaii, USA (Stratospheric)
- Lauder, New Zealand (Stratospheric)

Product time period: Jan 1 – Dec 31, 2014

Data provider: NDACC

Instrument provider: Various

Product assessor: Arnoud Apituley, KNMI

Assessor contact email: [apituley@knmi.nl](mailto:apituley@knmi.nl)

## 2.1 Guidance notes

For general guidance see the Guide to Uncertainty in Measurement & its Nomenclature, published as part of the GAIA-CLIM project.

This document is a measurement product technical document which should be stand-alone i.e. intelligible in isolation. Reference to external sources (preferably peer-reviewed) and documentation from previous studies is clearly expected and welcomed, but with sufficient explanatory content in the GAIA CLIM document not to necessitate the reading of all these reference documents to gain a clear understanding of the GAIA CLIM product and associated uncertainties entered into the Virtual Observatory (VO).

In developing this guidance, we have created a convention for the traceability identifier numbering as shown in Figure 1. The ‘main chain’ from raw measurand to final product forms the axis of the diagram, with top level identifiers (i.e. 1, 2, 3 etc.). Side branch processes add sub-level components to the top level identifier (for example, by adding alternate letters & numbers, or 1.3.2 style nomenclature).

**The key purpose of this sub-level system is that all the uncertainty from a sub-level are summed in the next level up.**

For instance, using Figure 1, contributors 2a1, 2a2 and 2a3 are all assessed as separate components to the overall traceability chain (have a contribution table). The contribution table for (and uncertainty associated with) 2a, should combine all the sub-level uncertainties (and any additional uncertainty intrinsic to step 2a). In turn, the contribution table for contributor 2, should include all uncertainties in its sub-levels.

Therefore, only the top level identifiers (1, 2, 3, etc.) shown in bold in the summary table need be combined to produce the overall product uncertainty. The branches can therefore be considered in isolation, for the more complex traceability chains, with the top level contribution table transferred to the main chain. For instance, see Figure 2 & Figure 3 as an example of how the chain can be divided into a number of diagrams for clearer representation.

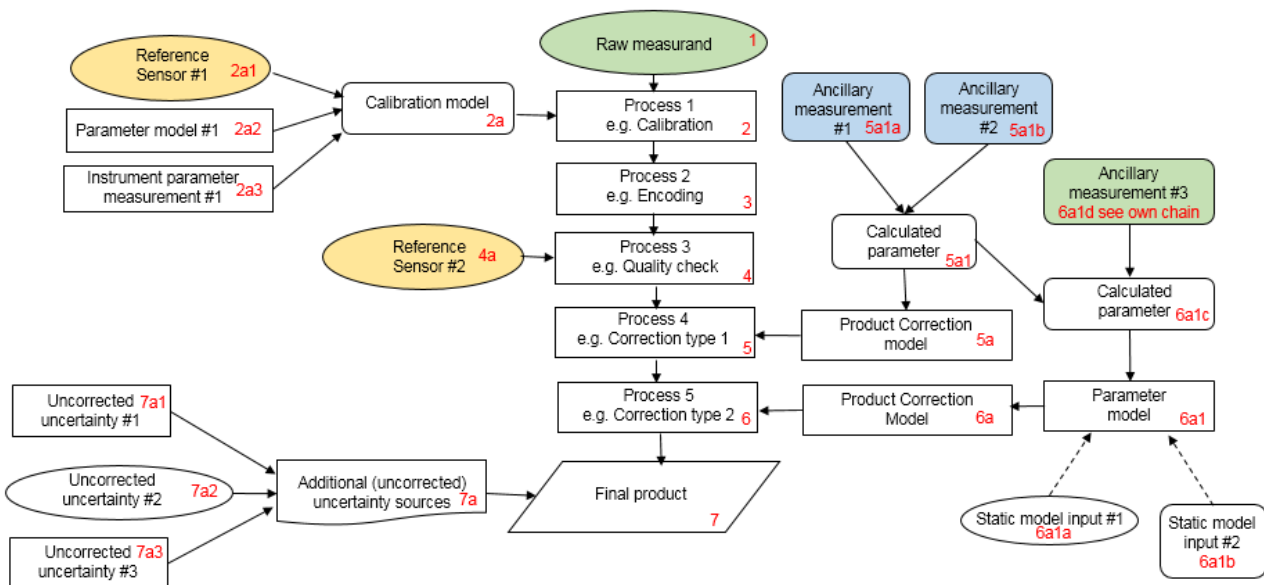


Figure 1. Example traceability chain. Green represents a key measurand or ancillary measurand recorded at the same time with the product raw measurand. Yellow represents a source of traceability. Blue represents a static ancillary measurement

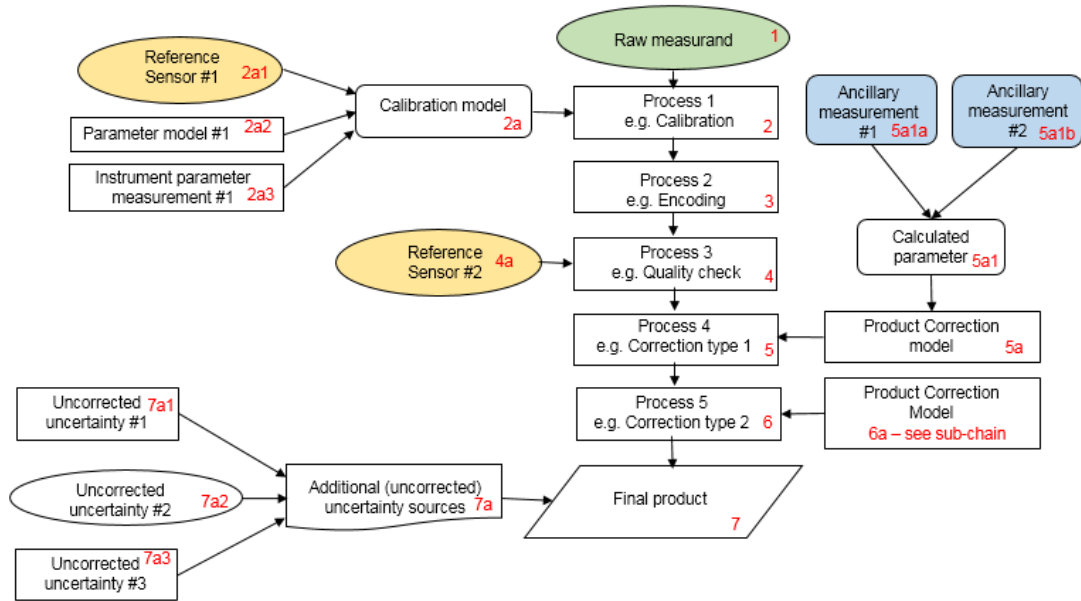


Figure 2. Example chain as sub-divided chain. Green represents a key measurand or ancillary measurand recorded at the same time with the product raw measurand. Yellow represents a source of traceability. Blue represents a static ancillary measurement

When deciding where to create an additional sub-level, the most appropriate points to combine the uncertainties of sub-contributions should be considered, with additional sub-levels used to illustrate where their contributions are currently combined in the described process.

A short note on colour coding. Colour coding can/should be used to aid understanding of the key contributors, but we are not suggesting a rigid framework at this time. In Figure 1, green represents a key measurand or ancillary or complementary measurand recorded at the same time with the raw measurand; yellow represents a primary source of traceability & blue represents a static ancillary measurement (site location, for instance). Any colour coding convention you use, should be clearly described.

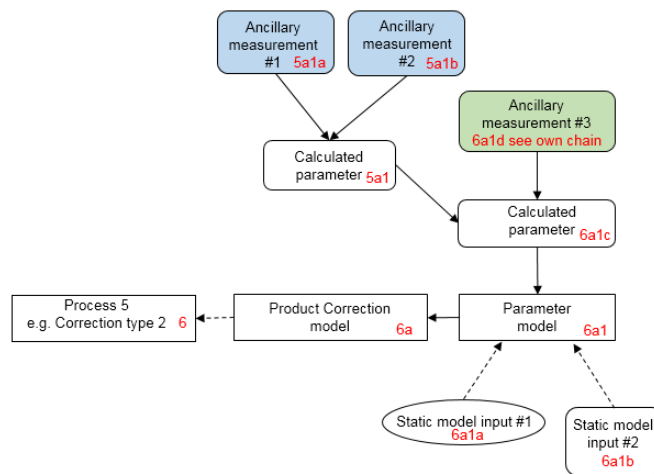


Figure 3. Example chain contribution 6a sub-chain. Green represents a key measurand or ancillary measurand recorded at the same time with the product raw measurand. Blue represents a static ancillary measurement

The contribution table to be filled for each traceability contributor has the form seen in Table 1.

Table 1. The contributor table.

Information / data	Type / value / equation	Notes / description
<b>Name of effect</b>		
<b>Contribution identifier</b>		
<b>Measurement equation parameter(s) subject to effect</b>		
<b>Contribution subject to effect (final product or sub-tree intermediate product)</b>		
<b>Time correlation extent &amp; form</b>		
<b>Other (non-time) correlation extent &amp; form</b>		
<b>Uncertainty PDF shape</b>		
<b>Uncertainty &amp; units</b>		
<b>Sensitivity coefficient</b>		
<b>Correlation(s) between affected parameters</b>		
<b>Element/step common for all sites/users?</b>		
<b>Traceable to ...</b>		
<b>Validation</b>		

**Name of effect** – The name of the contribution. Should be clear, unique and match the description in the traceability diagram.

**Contribution identifier** - Unique identifier to allow reference in the traceability chains.

**Measurement equation parameter(s) subject to effect** – The part of the measurement equation influenced by this contribution. Ideally, the equation into which the element contributes.

**Contribution subject to effect** – The top level measurement contribution affected by this contribution. This can be the main product (if on the main chain), or potentially the root of a side branch contribution. It will depend on how the chain has been sub-divided.

**Time correlation extent & form** – The form & extent of any correlation this contribution has in time.

**Other (non-time) correlation extent & form** – The form & extent of any correlation this contribution has in a non-time domain. For example, spatial or spectral.

**Uncertainty PDF shape** – The probability distribution shape of the contribution, Gaussian/Normal Rectangular, U-shaped, log-normal or other. If the form is not known, a written description is sufficient.

**Uncertainty & units** – The uncertainty value, including units and confidence interval. This can be

a simple equation, but should contain typical values.

**Sensitivity coefficient** – Coefficient multiplied by the uncertainty when applied to the measurement equation.

**Correlation(s) between affected parameters** – Any correlation between the parameters affected by this specific contribution. If this element links to the main chain by multiple paths within the traceability chain, it should be described here. For instance, SZA or surface pressure may be used separately in a number of models & correction terms that are applied to the product at different points in the processing. See Figure 1, contribution 5a1, for an example.

**Element/step common for all sites/users** – Is there any site-to-site/user-to-user variation in the application of this contribution?

**Traceable to** – Describe any traceability back towards a primary/community reference.

**Validation** – Any validation activities that have been performed for this element?

### 3 Introduction

This document presents the Product Traceability and Uncertainty (PTU) information for the ozone profile differential absorption lidar product. The aim of this document is to provide supporting information for the users of this product within the GAIA-CLIM VO. The uncertainty and traceability information contained in this document is based on the details given in LeBlanc et al. (2016b).

LeBlanc et al. (2016b) describe an approach for the definition, propagation, and reporting of uncertainty in the ozone differential absorption lidar data products contributing to the Network for the Detection of Atmospheric Composition Change (NDACC) database. One essential aspect of the proposed approach is the propagation in parallel of all independent uncertainty components through the data processing chain before they are combined together to form the ozone combined standard uncertainty.

The independent uncertainty components contributing to the overall budget include random noise associated with signal detection, uncertainty due to saturation correction, background noise extraction, the absorption cross sections of O<sub>3</sub>, NO<sub>2</sub>, SO<sub>2</sub>, and O<sub>2</sub>, the molecular extinction cross sections, and the number densities of the air, NO<sub>2</sub>, and SO<sub>2</sub>. The expression of the individual uncertainty components and their step-by-step propagation through the ozone differential absorption lidar (DIAL) processing chain are thoroughly estimated. All sources of uncertainty except detection noise imply correlated terms in the vertical dimension, which requires knowledge of the covariance matrix when the lidar signal is vertically filtered. In addition, the covariance terms must be taken into account if the same detection hardware is shared by the lidar receiver channels at the absorbed and non-absorbed wavelengths.

The ozone uncertainty budget is presented as much as possible in a generic form (i.e., as a function of instrument performance and wavelength) so that all NDACC ozone DIAL investigators across the network can estimate, for their own instrument and in a straightforward manner, the expected impact of each reviewed uncertainty component.

In the example of a stratospheric ozone DIAL after optimal combination of three DIAL wavelength pairs, the ozone number density standard uncertainty results mainly from three components: Rayleigh extinction cross section differential at the bottom of the profile, ozone absorption cross section differential in the middle of the profile, and detection noise at the top of the profile. For the derived ozone mixing ratio, the uncertainty component associated with the *a priori* use of ancillary air pressure can become abruptly important above 30 km as a result of the transition between the *a priori* use of radiosonde measurement ( $z < 30$  km) and the *a priori* use of the NCEP analysis ( $z > 30$  km). The dominant source of ozone mixing ratio uncertainty above 45 km is detection noise

## 4 Instrument description

The basic setup of a lidar system is shown in Fig.4. The lidar technique, acronym for ‘light detection and ranging’, is based on the transmission into the atmosphere of short light pulses, with duration ranging from a few to several hundreds of nanoseconds, by a laser transmitter, directly or by means of transmission optics. In any point of the atmospheric volume crossed by the laser beam, a portion of the incident light is backscattered by atmospheric constituents. This backscattered light is collected by a receiving telescope. The light received from the atmosphere passes through an optical system, consisting of various elements (lenses, mirrors, filters, etc.), which selects specific wavelengths of the light collected by the telescope. The light from the optical system is forwarded to detectors, typically photomultipliers that convert the light into electrical signals. An electronic trigger circuit synchronizes the data acquisition to start with the emission of each laser pulse so that atmospheric signals are acquired as a function of elapsed time with respect to the emission of each laser pulse, from which distance can be inferred unambiguously. These signals are the lidar signals, measuring the intensity of the light backscattered by the atmosphere as a function of the distance from the lidar.

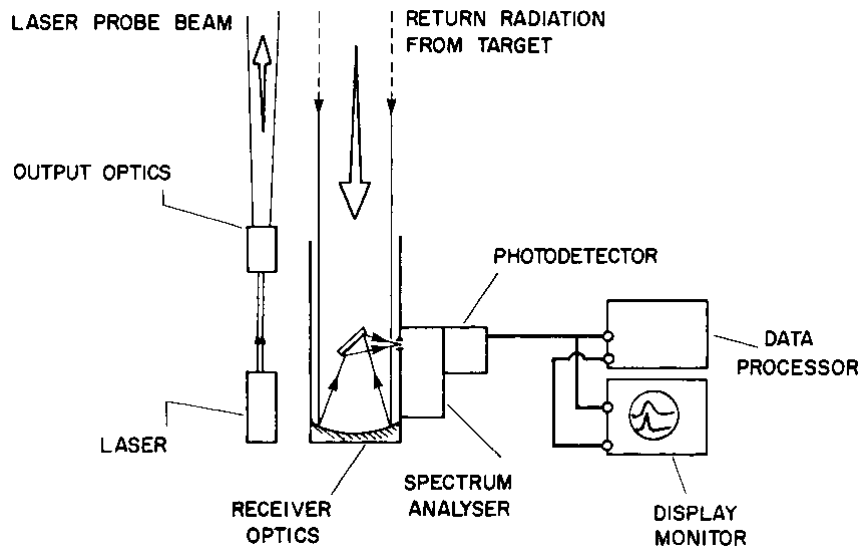


Fig. 4 Schematic of a basic vertically pointing lidar system (Measures, 1984)

To retrieve an ozone profile in the troposphere or stratosphere using the DIAL technique, we start from the Lidar Equation (e.g., Hinkley, 1976; Weitkamp, 2005). This equation in its most compressed form describes the emission of light by a laser source, its backscatter at altitude  $z$ , its extinction and scattering along its path up and back, and its collection back on a detector:

$$P(z, \lambda_E, \lambda_R) = P_L(\lambda_E) \frac{\xi(z, \lambda_R) \delta z}{(z - z_L)^2} \tau_{UP}(z, \lambda_E) \beta(z, \lambda_E, \lambda_R) \tau_{DOWN}(z, \lambda_R) \quad (1)$$

- $\lambda_E$  is the laser emission wavelength and  $\lambda_R$  is the receiver detection wavelength. Note that this subscript may change to indicate different wavelengths later on in the document;
- $P$  is the total number of photons collected at wavelength  $\lambda_R$  on the lidar detector surface;
- $\delta z$  is the thickness of the backscattering layer sounded during the time interval  $\delta t$  ( $\delta z = c\delta t/2$ , where  $c$  is the speed of light);
- $P_L$  is the number of photons emitted at the emission wavelength  $\lambda_E$  ;
- $\xi$  is the optical efficiency of the receiving channel, including optical and spectral transmittance and geometric obstruction;
- $z$  is the altitude of the backscattering layer;

- $z_L$  is the altitude of the lidar (laser and receiver assumed to be at the same altitude);
- $\beta$  is the total backscatter coefficient (including particulate  $\beta_P$  and molecular  $\beta_M$  backscatter);
- $\tau_{UP}$  is the optical thickness integrated along the outgoing beam path between the lidar and the scattering altitude  $z$ , and is defined as

$$\tau_{UP}(z) = \exp \left[ - \int_{z_L}^z \left( \sigma_M(\lambda_E) N_a(z') + \alpha_P(z', \lambda_E) + \sum_i \sigma_i(z', \lambda_E) N_i(z') \right) dz' \right] \quad (2)$$

- $\tau_{DOWN}$  is the optical thickness integrated along the returning beam path between the scattering altitude  $z$  and the lidar receiver, and is defined as

$$\tau_{DOWN}(z) = \exp \left[ - \int_{z_L}^z \left( \sigma_M(\lambda_R) N_a(z') + \alpha_P(z', \lambda_R) + \sum_i \sigma_i(z', \lambda_R) N_i(z') \right) dz' \right] \quad (3)$$

where  $\sigma_M$  is the molecular extinction cross section due to Rayleigh scattering (Strutt, 1899) (hereafter called “Rayleigh cross section” for brevity),  $N_a$  is the air number density,  $\alpha_P$  is the particulate extinction coefficient,  $\sigma_i$  is the absorption cross section of absorbing constituent  $i$ , and  $N_i$  is the number density of absorbing constituent  $i$ . For the altitude range of interest of the ozone DIAL measurements, the Rayleigh cross sections can be considered constant with altitude, and therefore depend only on wavelength. The absorption cross sections, however, are in most cases temperature-dependent, and should be taken as a function of both altitude and wavelength. In the DIAL technique we consider the lidar signals measured at two different wavelengths, the light at one wavelength being more absorbed by the target species (here, ozone) than the light at the other wavelength (Mégie et al., 1977). Using the notation ON for the most absorbed wavelength, and OFF for the least absorbed wavelength, Eq. (1) can be re-written for each of the emitted wavelength:

$$P_{ON}(z) = P_L(\lambda_1) \frac{\xi_{ON}(z) \delta z}{(z - z_L)^2} \tau_{UP}(z, \lambda_1) \beta(z, \lambda_1, \lambda_2) \tau_{DOWN}(z, \lambda_2) \quad (4)$$

$$P_{OFF}(z) = P_L(\lambda_3) \frac{\xi_{OFF}(z) \delta z}{(z - z_L)^2} \tau_{UP}(z, \lambda_3) \beta(z, \lambda_3, \lambda_4) \tau_{DOWN}(z, \lambda_4) \quad (5)$$

The emitted and received wavelength subscripts have been modified as follows:

$\lambda_1$  and  $\lambda_2$  are the emitted and received “ON” wavelengths respectively

$\lambda_3$  and  $\lambda_4$  are the emitted and received “OFF” wavelengths respectively

To obtain ozone number density  $N_{O_3}$ , Eqs. (4)–(5) are rearranged and subsequently the vertical derivative of the logarithm of the ratio of the lidar signals measured at the ON and OFF wavelengths (Mégie et al., 1977):

$$N_{O_3}(z) = \frac{1}{\Delta \sigma_{O_3}(z)} \left[ \frac{\partial}{\partial z} \left( \ln \frac{P_{OFF}(z)}{P_{ON}(z)} \right) - \Delta \sigma_M N_a(z) - \left( \sum_{ig} \Delta \sigma_{ig}(z) N_{ig}(z) \right) - \Delta \alpha_P(z) + \Lambda \eta(z) + \Lambda \beta(z) \right] \quad (6)$$

The ozone DIAL measurement model depends on the choice of the theoretical equations used as well as their implementation to the real world, i.e., after considering all the caveats associated with the design, setup, and operation of an actual lidar instrument. Equation (6) relates to the expected number of photons reaching the lidar detectors ( $P_{ON}$  and  $P_{OFF}$ ), not the actual raw lidar signals recorded in the data files by a real instrument. Its practical implementation for the retrieval of ozone therefore requires, on one hand the addition of several signal correction procedures and numerical transformations that depend on the instrumentation, and on the other hand, the development of

approximations and/or the adoption of assumptions aimed to reduce the complexity of the measurement model.

In this context, uncertainty components associated with particulate extinction and backscatter ( $\alpha_p$  and  $\beta$  terms in Eq. 6) will not be considered here. Their contribution is negligible in a cloud-free, “clean” atmosphere, which is mostly true for altitudes above 35 km (e.g., Godin-Beekmann et al., 2003), and in most cases of clear-sky, free-tropospheric ozone DIAL measurements for which the wavelength differential is small (Papayannis et al., 1990; McDermid et al., 2002). When present and non-negligible, the contribution of particulate extinction and backscatter is highly variable from site to site, time to time, and highly dependent on the nature and quantity of the particulate matter at the time of measurement. A number of rather different assessment methods exist (for a review, see e.g., Eisele and Trickl, 2005). Proposing a meaningful standardized treatment of this uncertainty component is therefore complex and beyond the scope of the present work.

Similarly, uncertainty due to incomplete beam-telescope overlap correction ( $\eta$  term in Eq. 6) is instrument-dependent and often time-dependent for the same instrument. Therefore, no standardized formulation is provided here. However an example of treatment is provided in the ISSI team report (Leblanc et al., 2016c).

The detectors quantum efficiencies and the effects of the data recorders (e.g., sky and electronic background noise, signal saturation) must be taken into account. Due to the diversity of lidar instrumentation, it is not possible to provide a single expression for the parametrization of these effects and obtain a unique, real-world version of Eq. (6) applicable to all systems. However, we use standardized expressions that characterize the most commonly found cases, with the idea that the proposed approach for the propagation of uncertainty can be similarly applied to other cases. Specifically, to transition from a theoretical to a real ozone DIAL measurement model, we apply the following transformations.

- For each lidar receiver channel, the actual raw signal  $R$  recorded in the data files is represented by a vector of discretized values rather than a continuous function of altitude range:  
 $z \rightarrow z(k)$  and  $R(z) \rightarrow R(k)$  for  $k = 1, nk$ .
- The actual raw signal recorded in the data files is a combination of laser light backscattered in the atmosphere, sky background light that can be parametrized by a constant offset, and noise generated within the electronics (dark current and possibly signal-induced noise) that can be parametrized by a linear or nonlinear function of time, i.e., altitude range.
- Only channels operating in photon-counting mode are considered hereafter. For analog channels, uncertainty due to analog-to-digital signal conversion needs to be estimated. This estimation is highly instrument-dependent, and no meaningful standardized recommendations can therefore be provided.
- In photon-counting detection mode, the recorded signals result from nonlinear transfer of the detected signals due to the inability of the counting electronics to temporally discriminate a very large number of photon-counts reaching the detector (“pulse pile-up” effect resulting in signal saturation) (e.g., Müller, 1973; Donovan et al., 1993). In the present work, we consider the most frequent case of non-paralyzable photon-counting systems (i.e., using “non-extended dead time”, Müller, 1973), which allows for an analytical correction of the pulse pile-up effect.
- The ozone DIAL measurement includes detection noise, and it is desirable to filter this noise whenever it is expected to impact the retrieved product. The filtering process impacts the propagation of uncertainties, and therefore should be included in the measurement model. For each individual altitude  $z(k)$ , the filtering process consists of convolving a set of filter coefficients  $c_p$  with an unsmoothed signal  $s_u$  to obtain a smoothed signal  $s_m$ .

Given the above numerical signal transformations, a discretized version of Eq. (6) can now be formulated as follows:

$$N_{O_3}(k) = \frac{1}{\Delta\sigma_{O_3}(k)} \left[ S(k) - \Delta\sigma_M N_a(k) - \left( \sum_{ig} \Delta\sigma_{ig}(k) N_{ig}(k) \right) \right] \quad (7)$$

A product commonly derived from the lidar-measured ozone number density is ozone mixing ratio  $q_{O_3}$ . The transformation simply consists of dividing the lidar-measured ozone number density by the “best available” ancillary air number density:

$$q_{O_3}(k) = \frac{1}{\Delta\sigma_{O_3}(k)} \left[ \frac{S(k)}{N_a(k)} - \Delta\sigma_M - \left( \sum_{ig} \Delta\sigma_{ig}(k) q_{ig}(k) \right) \right] \quad (8)$$

The instrumentation-related input quantities to consider in the ozone uncertainty budget, described here, based on the NDACC-lidar standardized proposed approach, are the following:

1. detection noise inherent to photon-counting signal detection;
2. saturation (pulse pile-up) correction parameters (typically, photon counters’ dead time  $\tau$ );
3. background noise extraction parameters (typically, fitting parameters for function B).

Based on Eqs. (7)–(8), the additional external input quantities to consider in the ozone uncertainty budget are the following:

4. ozone absorption cross sections differential  $\sigma_{O_3}$ ;
5. Rayleigh extinction cross sections differential  $\sigma_M$ ;
6. ancillary air number density profile  $N_a$  (or temperature  $T_a$  and pressure  $p_a$  profiles);
7. absorption cross sections differential for the interfering gases  $\sigma_{ig}$ ;
8. Number density profiles  $N_{ig}$  (or mixing ratio profile  $q_{ig}$ ) of the interfering species.

The interfering gases (ig) to consider in practice are  $NO_2$ ,  $SO_2$ , and  $O_2$ . Because of either very low concentrations or very low values of their absorption cross section differentials for the ON and OFF wavelengths typically used for stratospheric and tropospheric ozone DIAL, no other atmospheric gases or molecules are expected to interfere with the ozone DIAL retrieval. In addition,  $NO_2$  and  $SO_2$  absorption is usually negligible in the stratospheric ozone retrieval (0.1–1 % ozone uncertainty or less ~~if neglected~~), as well as most cases of tropospheric ozone retrieval. However it is included here to account for the potentially non-negligible effect of a heavily polluted boundary layer, or potentially heavy volcanic aerosols loading conditions (Godin-Beekmann et al., 2003). The absorption by  $O_2$  should be considered only if any of the detection wavelengths is shorter than 294 nm as the interfering absorption relates to the Herzberg continuum, Herzberg and Wulf bands (Jenouvrier et al., 1999; Fally et al., 2000; Merienne et al., 2001). As already mentioned, the  $O_2$  number density  $N_{O_2}$  is assumed to be directly proportional to air number density  $N_a$  (constant mixing ratio), and therefore should not be considered as an input quantity.

In order to limit the complexity of the standardization process, the contribution of uncertainty associated with the fundamental physical constants is treated differently from that of the other input quantities. We refer here to an internationally recognized and traceable standard for our recommendations on the use of physical constants, namely the International Council for Science (ICSU) Committee on Data for Science and Technology (CODATA, <http://www.codata.org/>), endorsed by the BIPM (Mohr et al., 2008). Within the CODATA, the Task Group on Fundamental Constants (TGFC) provides the scientific and technological communities a self-consistent set of internationally recommended values of the basic constants and conversion factors of physics and chemistry that can be found here: <http://physics.nist.gov/cuu/Constants/index.html>.

Our proposed approach ensures that there is indeed no propagation of uncertainty for fundamental physical constants. To do so, we truncate the CODATA reported values to the decimal level where the CODATA reported uncertainty no longer affects rounding.

## 5 Product Traceability Chain

The PTU is given below for ozone profile retrievals in the stratosphere and troposphere with DIAL. The PTU is divided into two sections: the physical model is presented in Figure 5 and the processing model in Figure 6. The numbered boxes in these figures indicate the key elements in the PTU chain that are the main contributors to the overall measurement uncertainty. Each of these elements is discussed in Section 6.

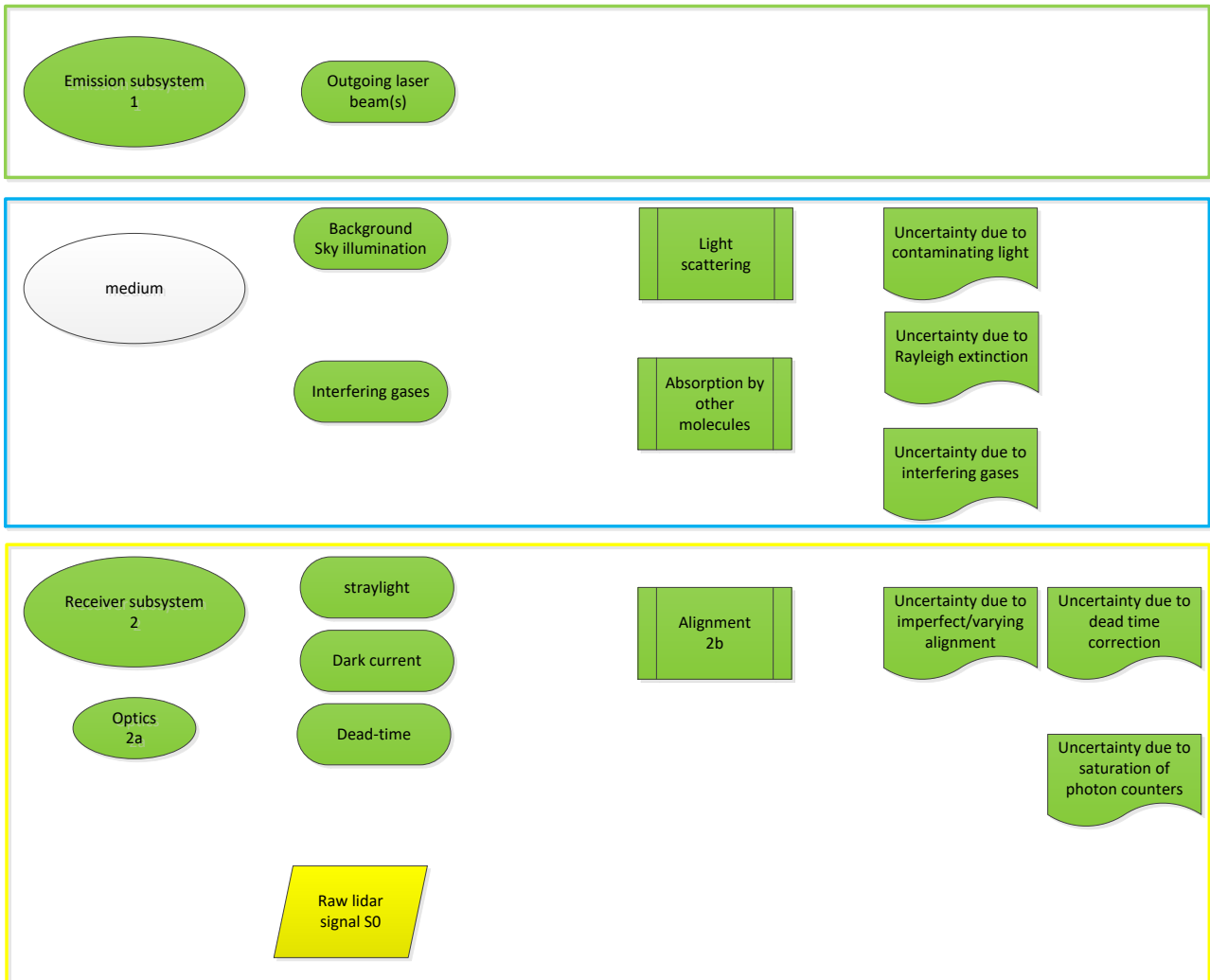


Figure 5. Four elements are shown in the physical part of the PTU chain: the emitter box (outlined by the green rectangle), the medium corresponding to the atmosphere (blue rectangle), the receiver box with e.g. the optics and detectors (yellow rectangle) and the processing software (orange rectangle on the following page). Processes and uncertainties that are considered in this document are shown as filled green shapes. Other sources of uncertainty have been listed, but are either, considered negligible, highly variable and therefore very hard to quantify, or avoidable (by proper technical design of the instrument).

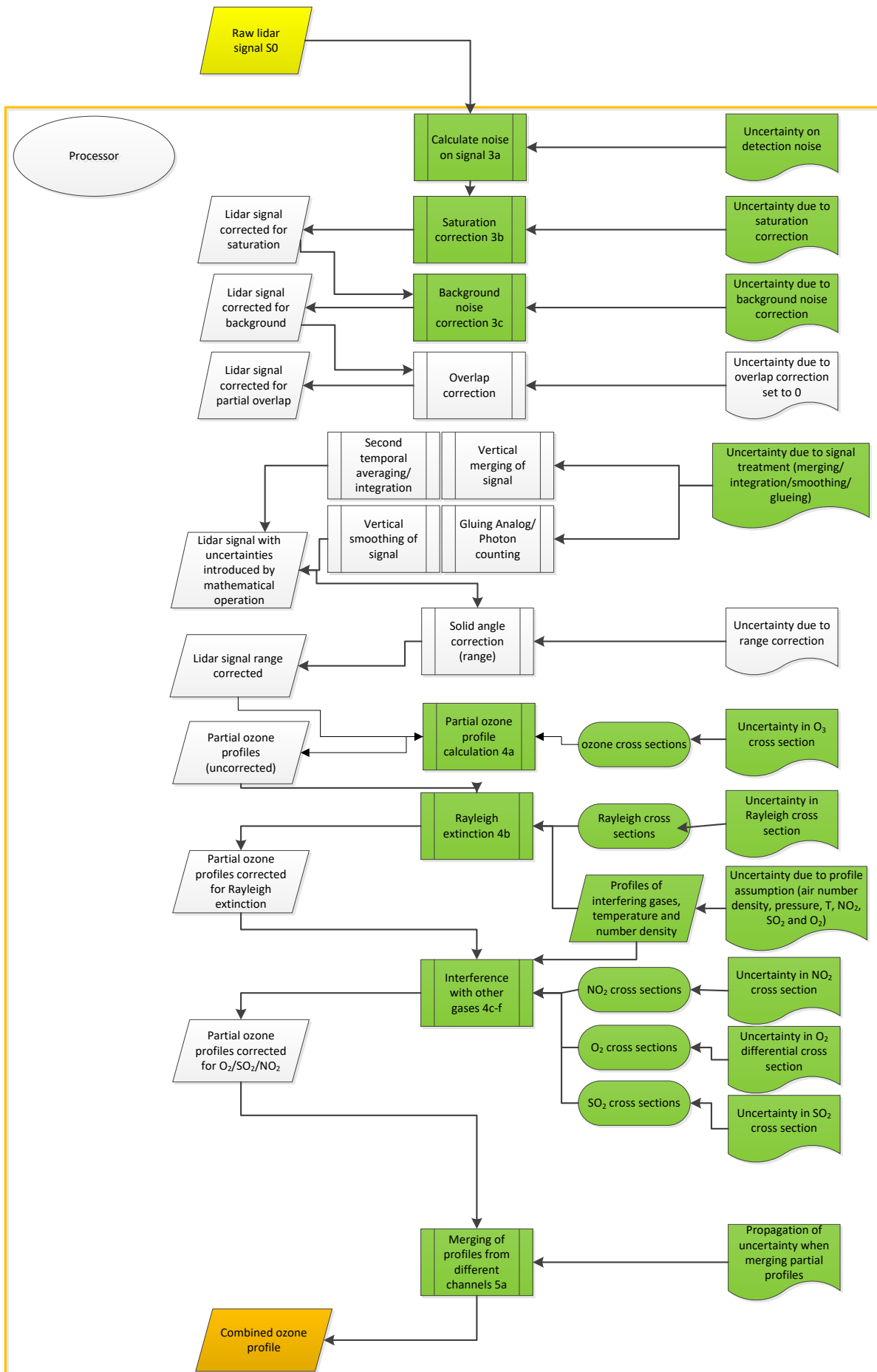


Figure 6. Flow chart of the data processing part of the PTU chain. The input originates from the lidar instrument for which the flow chart is depicted in Fig. 5.

## 6 Element contributions

### 6.1 Emission sub-system (1)

Light pulses at wavelengths  $\lambda_L = 308$  and  $353/355$  nm for stratospheric ozone DIAL and  $266, 277, 287, 289, 291, 299, 313$  and/or  $316$  nm for tropospheric ozone are sent out into the atmosphere by a laser transmitter directly or by means of transmission optics (mirrors, beam expander, etc.), and, if necessary, after Raman shifting to obtain another wavelength than the one produced by the laser. The parameters of the laser transmitter (pulse duration, energy and repetition rate, beam diameter and divergence) as well as of the transmission optics change are distinct for each lidar system. For this PTU, the distinction is that the stratospheric DIAL systems use larger telescopes (in the order of  $1$  m diameter) (McDermid, 1995), while the tropospheric lidars has a telescope with a diameter of about  $90$  cm and has several additional small receivers to cover the lowest ranges (McDermid, 2002). Changes over time due to aging and replacement of components, as well as responses to temperature changes may cause these parameters to change. These variations affect the optical power transmitted into the atmosphere.

Information / data	Type / value / equation	Notes / description
<b>Name of effect</b>	Transmission system	Contribution of variations in all the parameters related to the laser beam transmission to the atmosphere.
<b>Contribution identifier</b>	1	
<b>Measurement equation parameter(s) subject to effect</b>	$P_L$ and $\xi(\lambda_{ON}, \lambda_{OFF})$ in lidar equation	
<b>Contribution subject to effect (final product or sub-tree intermediate product)</b>	Lidar signal	
<b>Time correlation extent &amp; form</b>	Various time scales	Extent & form not quantified
<b>Other (non-time) correlation extent &amp; form</b>	1) Possible correlation with vertical range (if pulse duration increases so as to exceed the dwell time); 2) Possible correlation with the temperature of laser and transmission optics during measurements	Extent & form not quantified
<b>Uncertainty PDF shape</b>	N/A	Systematic effect
<b>Uncertainty &amp; units</b>	0% (relative uncertainty)	(Assumed to be negligible)
<b>Sensitivity coefficient</b>	$< 1$	(Assumed to be negligible)
<b>Correlation(s) between affected parameters</b>	None	
<b>Element/step common for all sites/users?</b>	Yes	
<b>Traceable to ...</b>	N/A	
<b>Validation</b>	N/A	

## 6.2 Receiving sub-system (2)

The portion of the laser radiation backscattered by the atmosphere at different altitude ranges is collected by a telescope. For tropospheric ozone DIAL the best suitable wavelengths to be used are below 300 nm. For stratospheric ozone DIAL, wavelengths longer than 300 nm are used. Two or more telescopes with different collecting apertures are usually employed to optimally cover the signal dynamic range (near range, far range). The radiation collected by the telescope passes through an optical system (consisting of lenses, mirrors, filters, beam splitters and interference filters) where it is spectrally filtered, so only backscattered light at the ON and OFF wavelengths are transmitted to the detection system. The uncertainty contribution of the receiving system is the combination of contributions related to the receiver optical parameters (2a) and the alignment of the lidar system (2b), whose uncertainties and correlation effects are described in the corresponding sub-level sections.

Information / data	Type / value / equation	Notes / description
<b>Name of effect</b>	Receiving system	Combined contribution of the receiver optical parameters (2a) and alignment of the lidar system (2b)
<b>Contribution identifier</b>	2	
<b>Measurement equation parameter(s) subject to effect</b>	$\xi(\lambda_L, \lambda_S)$ in lidar equation	
<b>Contribution subject to effect (final product or sub-tree intermediate product)</b>	Ozone profile $\text{NO}_3(z)$	
<b>Time correlation extent &amp; form</b>	Various time scales	Extent & form not quantified
<b>Other (non-time) correlation extent &amp; form</b>	May affect vertical correlation	
<b>Uncertainty PDF shape</b>	N/A	Systematic effect
<b>Uncertainty &amp; units</b>	0% (relative uncertainty) combination of 2a and 2b	Assumed to be negligible
<b>Sensitivity coefficient</b>	1	
<b>Correlation(s) between affected parameters</b>	None	
<b>Element/step common for all sites/users?</b>	Yes	
<b>Traceable to ...</b>	N/A	
<b>Validation</b>	N/A	

### 6.3 Receiver optical parameters (2a)

The optical properties of the elements forming the receiver, consisting of the telescope and the following optical filtering system, change depending on the lidar system, but they may also change for a given lidar system due to their time and temperature instability, contamination, or to the replacement of one or more components of the receiving system. These variations in the parameters of the receiving system affect the optical power transmitted by the receiver to the detectors and therefore both the power and the random uncertainty of the signals used for the retrieval of ozone profiles. However, for well maintained instruments, quality assurance procedures are implemented (particularly in networks such as NDACC) and these variations are monitored and minimized (e.g., the optics are regularly cleaned, lidars usually operate in air-conditioned environments), so that their contribution to the retrieval and uncertainty of aerosol extinction coefficient profile is assumed to be negligible.

Information / data	Type / value / equation	Notes / description
<b>Name of effect</b>	Receiver optical parameters	Contribution of variations in all the optical parameters of the receiving system
<b>Contribution identifier</b>	2a	
<b>Measurement equation parameter(s) subject to effect</b>	$\xi(\lambda_{ON}, \lambda_{OFF})$	
<b>Contribution subject to effect (final product or sub-tree intermediate product)</b>	Lidar signals P <sub>ON</sub> and P <sub>OFF</sub>	
<b>Time correlation extent &amp; form</b>	Various time scales	Extent & form not quantified
<b>Other (non-time) correlation extent &amp; form</b>	1) Possible correlation with vertical range due to the correlation of the optical efficiency of the receiving system with the incident angle of backscattered light and, consequently, with the vertical range; 2) Possible correlation with the temperature of the receiver components during measurements	Extent & form not quantified
<b>Uncertainty PDF shape</b>	N/A	Systematic effect
<b>Uncertainty &amp; units</b>	0% (relative uncertainty)	(Assumed to be negligible)
<b>Sensitivity coefficient</b>	< 1	Assumed that only data not effected is reported
<b>Correlation(s) between affected parameters</b>	None	
<b>Element/step common for all sites/users?</b>	Yes	
<b>Traceable to ...</b>	N/A	
<b>Validation</b>	N/A	

## 6.4 Alignment (2b)

The correct alignment of the lidar system, that is the alignment of the laser beam with the receiving system and of the telescope with the optics of filtering system, is ensured by specific tests, as for instance developed in the frame of EARLINET quality assurance program. In particular, the so-called telecover test and the Rayleigh fit test are performed to check and correct the alignment of the lidar system in the near range (planetary boundary layer) and in the far range (free troposphere or above), respectively – see Freudenthaler (AMTD, 2018).

For each lidar system there is a certain degree of misalignment between the laser beam and the receiving system due to residual uncertainties in the telecover and Rayleigh fit tests or possible mechanical/thermal instabilities of the optical and mechanical components forming both transmission and receiving systems. The misalignment of a lidar system changes the angle on the receiver of the backscattered light at each altitude level, which affects the overlap function. For the DIAL application, there may be configurations that use multiple (two or more) outgoing laser beams that have to be co-aligned with one or more receivers. This gives rise to multiple overlap functions: one overlap function for each laser beam and associated detection channel. This implies a minimum overlap height for each of these overlap functions. For the DIAL technique to be reliably applied, only the data points originating from above the overlap function with the maximum overlap range should be applied. For the application of the DIAL technique, technical provisions should be in place to determine proper alignment, so that the minimum distance for data analysis can be determined. The minimum distance amounts to less than 10 km for stratospheric ozone lidars and less than 3 km for tropospheric ozone lidar.

Information / data	Type / value / equation	Notes / description
<b>Name of effect</b>	Alignment	
<b>Contribution identifier</b>	2b	
<b>Measurement equation parameter(s) subject to effect</b>	$\xi(\lambda_{ON}, \lambda_{OFF})$	
<b>Contribution subject to effect (final product or sub-tree intermediate product)</b>	Lidar signals $P_{ON}$ and $P_{OFF}$	
<b>Time correlation extent &amp; form</b>	Various time scales	Extent & form not quantified
<b>Other (non-time) correlation extent &amp; form</b>	1) Possible correlation with vertical range due to the correlation of $O(z)$ and optical efficiency of the receiving system with the vertical range; 2) Possible correlation with the temperature of components forming both transmission and receiving systems during measurements	Extent & form not quantified
<b>Uncertainty PDF shape</b>	N/A	Systematic effect
<b>Uncertainty &amp; units</b>	0% (relative uncertainty)	Assumed to be negligible
<b>Sensitivity coefficient</b>	<1	Assumed that only data not effected is reported

<b>Correlation(s) between affected parameters</b>	None	
<b>Element/step common for all sites/users?</b>	Yes	
<b>Traceable to ...</b>	No	
<b>Validation</b>	No	

## 6.5 Pre-processing (3)

### 6.5.1 Detection noise (3a)

Random noise is inherently present in any physical system performing an actual measurement. In the case of the ozone DIAL measurement, it is introduced at the detection level, where the signal is recorded in the data files (raw signal  $R$ ). The associated detection noise uncertainty is derived from Poisson statistics associated with the probability of detection of a repeated random event (Type A uncertainty estimation) (e.g., Measures, 1984). Using the subscript (DET) for detection noise, the uncertainty in the raw signal  $R$  owing to detection noise can be expressed independently for each altitude bin  $k$  and for each of the ON and OFF receiver channels by the square root of the raw signal assuming shot noise limited detector performance.

This uncertainty component reflects purely random effects, and therefore implies no correlation between any of the samples considered. We do not consider the case of instruments that (partially) share the same detection electronics, which would require formulating propagation of correlated uncertainties. In the latter case of correlated uncertainties, identical behavior for the ON and OFF channels would have to be assumed. The uncertainty is therefore propagated to ozone number density by consistently adding in quadrature the uncertainties of the individual samples used in the signal transformations. If we assume a non-paralyzable photon-counting hardware, it is propagated to the saturation and background noise corrected signal without covariance terms (LeBlanc, 2016b):

$$u_{PON(DET)}(k) = \left( \frac{P_{ON}(k)}{R_{ON}(k)} \right)^2 \sqrt{R_{ON}(k)} \quad (9)$$

$$u_{POFF(DET)}(k) = \left( \frac{P_{OFF}(k)}{R_{OFF}(k)} \right)^2 \sqrt{R_{OFF}(k)} \quad (10)$$

It is finally propagated to the retrieved ozone number density  $N_{O_3}$  and mixing ratio  $q_{O_3}$  without covariance terms:

$$u_{NO_3(DET)}(k) = \frac{1}{|\Delta\sigma_{O_3}(k)|\delta z} \sqrt{\sum_{p=-n}^n c_p^2(k) \left( \left( \frac{u_{PON(DET)}(k+p)}{P_{ON}(k+p)} \right)^2 + \left( \frac{u_{POFF(DET)}(k+p)}{P_{OFF}(k+p)} \right)^2 \right)} \quad (11)$$

$$u_{qO_3(DET)}(k) = \frac{1}{N_a(k)|\Delta\sigma_{O_3}(k)|\delta z} \sqrt{\sum_{p=-n}^n c_p^2(k) \left( \left( \frac{u_{PON(DET)}(k+p)}{P_{ON}(k+p)} \right)^2 + \left( \frac{u_{POFF(DET)}(k+p)}{P_{OFF}(k+p)} \right)^2 \right)} \quad (12)$$

Information / data	Type / value / equation	Notes / description
<b>Name of effect</b>	Detection noise	
<b>Contribution identifier</b>	3a	
<b>Measurement equation parameter(s) subject to effect</b>	S	Eq. 7, 8
<b>Contribution subject to effect (final product or sub-tree intermediate product)</b>	N <sub>O3</sub> , q <sub>O3</sub>	Eq. 7, 8
<b>Time correlation extent &amp; form</b>	Various time scales	Will change with each measurement session due to varying experimental conditions
<b>Other (non-time) correlation extent &amp; form</b>	Vertical smoothing/spatial resolution	
<b>Uncertainty PDF shape</b>	Poisson/normal	
<b>Uncertainty &amp; units</b>	0.1-100%	From near surface to maximum altitude, depending on vertical smoothing and spatial resolution
<b>Sensitivity coefficient</b>	1	
<b>Correlation(s) between affected parameters</b>	N/A	
<b>Element/step common for all sites/users?</b>	Yes	
<b>Traceable to ...</b>	Leblanc et al., 2016c	
<b>Validation</b>	Simeonov et al., 1999	

### 6.5.2 Saturation (pulse pile-up) correction (3b)

This uncertainty component is introduced only for channels operating in photon-counting mode. If we consider a non-paralyzable counting hardware, the only input quantity to introduce is the hardware's dead time (sometimes called resolving time), which characterizes the speed of the counting electronics. The dead time  $\tau$  and its uncertainty  $u_\tau$  are generally among the technical specifications provided by the hardware manufacturer (Type-B estimation).

The photon-counting hardware of the ON and OFF channels is different, so the channels can be considered independent and the saturation correction uncertainty can be propagated to the retrieved ozone number density and mixing ratio through the differentiation equation (Eqs.7-8), assuming no correlation between samples measured in the ON and OFF channels (no covariance terms), thus resulting in the following expressions:

$$u_{NO3(SAT)}(k) = \frac{1}{|\Delta\sigma_{O3}(k)|\delta_z} \sum_{p=-n}^n c_p(k) \sqrt{\left( \left( \frac{u_{PON(SAT)}(k+p)}{P_{ON}(k+p)} \right)^2 + \left( \frac{u_{POFF(SAT)}(k+p)}{P_{OFF}(k+p)} \right)^2 \right)} \quad (13)$$

$$u_{qO3(SAT)}(k) = \frac{1}{N_a(k)|\Delta\sigma_{O3}(k)|\delta_z} \sum_{p=-n}^n c_p(k) \sqrt{\left( \left( \frac{u_{PON(SAT)}(k+p)}{P_{ON}(k+p)} \right)^2 + \left( \frac{u_{POFF(SAT)}(k+p)}{P_{OFF}(k+p)} \right)^2 \right)} \quad (14)$$

Information / data	Type / value / equation	Notes / description
<b>Name of effect</b>	Saturation correction	
<b>Contribution identifier</b>	3b	
<b>Measurement equation parameter(s) subject to effect</b>	S	Eq. 7, 8
<b>Contribution subject to effect (final product or sub-tree intermediate product)</b>	N <sub>O3</sub> , q <sub>O3</sub>	Eq. 7, 8
<b>Time correlation extent &amp; form</b>	Various time scales	Will change with each measurement session due to varying experimental conditions
<b>Other (non-time) correlation extent &amp; form</b>	N/A	
<b>Uncertainty PDF shape</b>	Poisson/normal	
<b>Uncertainty &amp; units</b>	Tropospheric ozone: 20% near the surface, nonlinearly decreasing with altitude to near 0, when switching to other channel jumping to a smaller peak, followed by the nonlinear decrease with altitude For stratospheric ozone it works similarly, except that the maximum is about 1%	From near surface to maximum altitude
<b>Sensitivity coefficient</b>	1	
<b>Correlation(s) between affected parameters</b>	N/A	
<b>Element/step common for all sites/users?</b>	Yes	
<b>Traceable to ...</b>	Leblanc et al., 2016c	
<b>Validation</b>	Donovan et al, 2003 Bristow, 1998	

### 6.5.3 Background noise extraction (3c)

At far range (over 100 km range), the backscattered signal is too weak to be detected and any non-zero signal reflects the presence of undesired skylight or electronic background noise. This noise is typically subtracted from the total signal by fitting the uppermost part of the lidar signal with a linear or non-linear function of altitude  $B$ . A new uncertainty component associated with the noise fitting procedure must therefore be introduced. Here we provide a detailed treatment for the simple case of a linear fit. It can be easily generalized to many other fitting functions. The linear fitting function takes the form:

$$B(k) = b_0 + b_1 z(k) \quad (15)$$

For many well-known fitting methods (e.g., least-squares), the fitting coefficients  $b_i$  can be calculated analytically together with their uncertainty  $u_{b_i}$  and their correlation coefficient  $r_{b_i, b_j}$

(Type-A estimation) (Press et al., 1986). Using the subscript “(BKG)” for “background noise”, the background noise correction uncertainty is expressed independently for the ON and OFF channels we obtain:

$$u_{PON(BKG)}(k) = \sqrt{u_{b0\_ON}^2 + u_{b1\_ON}^2 z^2(k) + 2z(k)u_{b0\_ON}u_{b1\_ON}r_{b0,b1\_ON}} \quad (16)$$

$$u_{POFF(BKG)}(k) = \sqrt{u_{b0\_OFF}^2 + u_{b1\_OFF}^2 z^2(k) + 2z(k)u_{b0\_OFF}u_{b1\_OFF}r_{b0,b1\_OFF}} \quad (17)$$

The above two equations can be derived analytically for any fitting function for which the fitting method allows for the proper estimation of the fitting parameters’ covariance matrix (e.g., least-squares and singular value decomposition).

Because of the nature of the background noise correction (parameters  $b_i$  are independent of altitude), the approach used for the propagation of saturation correction uncertainty can also be used for the propagation of background noise correction uncertainty. In other words since the data acquisition hardware of the ON and OFF channels are different, the background noise correction uncertainty can be propagated assuming no correlation between the ON and OFF channels (no covariance terms):

$$u_{NO3(BKG)}(k) = \frac{1}{|\Delta\sigma_{O3}(k)|\delta z} \sum_{p=-n}^n c_p(k) \sqrt{\left(\frac{u_{PON(BKG)}(k+p)}{P_{ON}(k+p)}\right)^2 + \left(\frac{u_{POFF(BKG)}(k+p)}{P_{OFF}(k+p)}\right)^2} \quad (18)$$

$$u_{qO3(BKG)}(k) = \frac{1}{N_a(k)|\Delta\sigma_{O3}(k)|\delta z} \sum_{p=-n}^n c_p(k) \sqrt{\left(\frac{u_{PON(BKG)}(k+p)}{P_{ON}(k+p)}\right)^2 + \left(\frac{u_{POFF(BKG)}(k+p)}{P_{OFF}(k+p)}\right)^2} \quad (19)$$

The order of magnitude of the propagated ozone uncertainty due to background noise correction depends on many factors, including the relative magnitude of the ON and OFF signals with respect to noise being subtracted, and the slope of the signal-induced noise if signal-induced noise is present.

Having a constant noise and the case of noise having a well-known, small constant slope are the simplest cases to deal with, for which the only uncertainty component to consider is that due to the fitting parameters. In the presence of non-negligible signal-induced noise, the slope of the noise is no longer constant with altitude, and the background correction becomes much more uncertain. The uncertainty associated with non-linear fits is typically larger than that associated with a linear fit, but most importantly, the actual altitude dependence of the signal-induced noise is usually unknown, and an additional uncertainty component that cannot be quantified accurately should be introduced. For this reason, it is strongly recommended to design lidar receivers in such a way that no signal—induced noise is present at all. For the systems under consideration, this is assumed to be the case.

Information / data	Type / value / equation	Notes / description
<b>Name of effect</b>	Background Noise Extraction	
<b>Contribution identifier</b>	3c	
<b>Measurement equation parameter(s) subject to effect</b>	S	Eq. 7, 8
<b>Contribution subject to effect (final product or sub-tree intermediate product)</b>	NO <sub>3</sub> , qO <sub>3</sub>	Eq. 7, 8

<b>Time correlation extent &amp; form</b>	Various time scales	Will change with each measurement session due to varying experimental conditions, e.g. sky brightness (sun, moon, stars)
<b>Other (non-time) correlation extent &amp; form</b>	N/A	
<b>Uncertainty PDF shape</b>	Poisson/normal	
<b>Uncertainty &amp; units</b>	Tropospheric ozone: 1% at top of partial profiles, decreasing with signal strength to <0.1% For stratospheric ozone 1% near top of profile and decreasing below, negligible in the troposphere	From near surface to maximum altitude
<b>Sensitivity coefficient</b>	1	
<b>Correlation(s) between affected parameters</b>	N/A	
<b>Element/step common for all sites/users?</b>	Yes	
<b>Traceable to ...</b>	Leblanc et al., 2016c	
<b>Validation</b>	McDermid et al., 1990; McGee et al., 1995	

## 6.6 External inputs (4)

### 6.6.1 Ozone absorption cross section differential (4a)

When the uncertainty due to the ozone absorption cross-section differential is computed, the actual magnitude of this uncertainty can be very different depending on the type of backscatter (Rayleigh or Raman), and depending on the source of ozone absorption cross-section used. Temperature-dependent ozone absorption cross-sections values originate from various published works by spectroscopy groups around the world (e.g., Serdyuchenko et al., 2014; Bass and Paur, 1984; Bogumil et al., 2003; Chehade et al., 2013; Daumont et al., 1992; Brion et al., 1998; Burrows et al., 1999). These groups usually provide at least one type of uncertainty estimates associated with the cross-section values. Occasionally, they provide separate components due to systematic and random effects. If present, these two components are not introduced and propagated similarly. To account for this distinction, the subscripts “*R*” (for “random”) and “*S*” (for “systematic”) will be used hereafter whenever needed. Expressions for the ozone uncertainty due to the absorption cross-section differential are now provided for four common cases that are relevant to the suggested data sets.

#### 6.6.1.1 Random component

In this case, the random component of the cross-sections uncertainty  $u_{\sigma O_3}$  is used to derive the random component of the cross-section differential uncertainty (no covariance terms).

- Applied to the DIAL equation (**Eq. (7)**) assuming no covariance terms from the cross-section differential. For Rayleigh backscatter DIAL systems, the corresponding component is propagated to ozone number density and mixing ratio using:

$$u_{NO_3(\Delta\sigma_{O_3R})}(k) = \frac{2N_{O_3}(k)}{|\Delta\sigma_{O_3}(k)|} \sqrt{u_{\sigma_{O_3-1(R)}}^2(k) + u_{\sigma_{O_3-3(R)}}^2(k)} \quad (20)$$

$$u_{q_{O_3(\Delta\sigma_{O_3R})}}(k) = \frac{2q_{O_3}(k)}{|\Delta\sigma_{O_3}(k)|} \sqrt{u_{\sigma_{O_3-1(R)}}^2(k) + u_{\sigma_{O_3-3(R)}}^2(k)} \quad (21)$$

- For Raman backscatter DIAL systems, this uncertainty component is propagated to ozone number density and mixing ratio using:

$$u_{NO_3(\Delta\sigma_{O_3R})}(k) = \frac{N_{O_3}(k)}{|\Delta\sigma_{O_3}(k)|} \sqrt{u_{\sigma_{O_3-1(R)}}^2(k) + u_{\sigma_{O_3-2(R)}}^2(k) + u_{\sigma_{O_3-3(R)}}^2(k) + u_{\sigma_{O_3-4(R)}}^2(k)} \quad (22)$$

$$u_{q_{O_3(\Delta\sigma_{O_3R})}}(k) = \frac{q_{O_3}(k)}{|\Delta\sigma_{O_3}(k)|} \sqrt{u_{\sigma_{O_3-1(R)}}^2(k) + u_{\sigma_{O_3-2(R)}}^2(k) + u_{\sigma_{O_3-3(R)}}^2(k) + u_{\sigma_{O_3-4(R)}}^2(k)} \quad (23)$$

#### 6.6.1.2 Systematic component

The cross-sections uncertainty component due to systematic effects is not always present or reported. It is most often estimated by comparing several cross-section datasets and observing biases between those datasets. The expression for the propagation of this component depends on the degree of correlation between the datasets used. Here we consider only two cases: when a unique source of cross-section is used for all wavelengths (i.e., dataset originating from a single set of laboratory measurements), and when two independent cross-section datasets are used for the ON and OFF wavelengths.

- In the first case, applicable to the selected case study instruments, it is assumed that the same dataset is used for the absorption cross-sections at all wavelengths. The systematic component of the cross-sections uncertainty  $u_{\sigma_{O_3(S)}}$  is used to derive a systematic component of the cross-section differential’s uncertainty  $u_{\Delta\sigma_{O_3(S)}}$  assuming full correlation between all wavelengths. In this case the same expression holds for both Rayleigh and Raman backscatter channels:

$$u_{NO3(\Delta\sigma_{O3})}(k) = \frac{N_{O3}(k)}{|\Delta\sigma_{O3}(k)|} \left| u_{\sigma_{O3\_1(S)}}(k) + u_{\sigma_{O3\_2(S)}}(k) - u_{\sigma_{O3\_3(S)}}(k) - u_{\sigma_{O3\_4(S)}}(k) \right| \quad (24)$$

$$u_{qO3(\Delta\sigma_{O3})}(k) = \frac{q_{O3}(k)}{|\Delta\sigma_{O3}(k)|} \left| u_{\sigma_{O3\_1(S)}}(k) + u_{\sigma_{O3\_2(S)}}(k) - u_{\sigma_{O3\_3(S)}}(k) - u_{\sigma_{O3\_4(S)}}(k) \right| \quad (25)$$

- In the second case, it is assumed that two independent datasets are used for the cross-sections at the ON and OFF wavelengths. Though usually not the case, this situation can occur because laboratory studies often focus on specific spectral regions, not necessarily covering all the wavelengths in use by a particular DIAL system. With the assumption of two independent cross-section datasets, the systematic component of the cross-sections uncertainty reported by both datasets is assumed randomized (Type-B estimation). Therefore the uncertainty component due to systematic effects should be propagated assuming that 1) the cross-section values used within the same dataset are fully correlated, and 2) none of cross-section values of one dataset is correlated with a cross-section value of the other dataset. The resulting ozone uncertainty component can then be written for both Rayleigh and Raman backscatter channels:

$$u_{NO3(\Delta\sigma_{O3})}(k) = \frac{N_{O3}(k)}{|\Delta\sigma_{O3}(k)|} \sqrt{\left( u_{\sigma_{O3\_1(S)}}(k) + u_{\sigma_{O3\_2(S)}}(k) \right)^2 + \left( u_{\sigma_{O3\_3(S)}}(k) + u_{\sigma_{O3\_4(S)}}(k) \right)^2} \quad (26)$$

$$u_{qO3(\Delta\sigma_{O3})}(k) = \frac{q_{O3}(k)}{|\Delta\sigma_{O3}(k)|} \sqrt{\left( u_{\sigma_{O3\_1(S)}}(k) + u_{\sigma_{O3\_2(S)}}(k) \right)^2 + \left( u_{\sigma_{O3\_3(S)}}(k) + u_{\sigma_{O3\_4(S)}}(k) \right)^2} \quad (27)$$

In **Eqs. (24)-(27)**, the Rayleigh backscatter case simply consists of replacing subscripts “3” and “4” by “1” and “2” respectively.

Equations (20)-(27) show that the relative uncertainty in the retrieved ozone is directly proportional to the relative uncertainty in the ozone absorption cross-section, which makes this latter factor the main source of uncertainty in the nominal measurement region of the ozone DIAL method (Godin-Beekmann and Nair, 2012). For stratospheric ozone DIAL pairs (308/355 and 332/387), the absorption cross-section at the “ON” wavelength is much larger than that at the “OFF” wavelength, resulting in an ozone relative uncertainty mostly dominated by the absorption cross-section uncertainty at the “ON” wavelength, and therefore leading to approximate 1-to-1 relationship between the ozone number density relative uncertainty and the absorption cross-section relative uncertainty. For tropospheric ozone DIAL pairs (299/316, 289/299, 266/289, and 287/294), the absorption cross-sections at the “ON” and “OFF” wavelengths are closer to each other. As a result, the curves depart slightly from the 1-1 relation observed for the stratospheric pairs. A 1-to-1 relationship is also observed for the all-systematic case as a result of the linear combination of **Eqs. (26)-(27)**.

Information / data	Type / value / equation	Notes / description
<b>Name of effect</b>	Ozone absorption cross section differential	
<b>Contribution identifier</b>	4a	
<b>Measurement equation parameter(s) subject to effect</b>	$\Delta\sigma_{O3}$	Eq. 7, 8
<b>Contribution subject to effect (final product or sub-tree intermediate product)</b>	$N_{O3}, q_{O3}$	Eq. 7, 8
<b>Time correlation extent &amp; form</b>	None	

<b>Other (non-time) correlation extent &amp; form</b>	None	
<b>Uncertainty PDF shape</b>	Unknown	Random and Systematic
<b>Uncertainty &amp; units</b>	2% for stratospheric ozone, 4-6% for tropospheric ozone depending on wavelengths used	Constant with altitude for number density and wavelength pair
<b>Sensitivity coefficient</b>	1	
<b>Correlation(s) between affected parameters</b>	N/A	
<b>Element/step common for all sites/users?</b>	No	No community consensus about consistent use of cross sections.
<b>Traceable to ...</b>	Leblanc et al., 2016c	
<b>Validation</b>	Godin-Beekmann and Nair, 2012	

### 6.6.2 Rayleigh extinction cross section differential (4b)

An approach similar to that used for the ozone absorption cross-section differential uncertainty can be used for the Rayleigh extinction cross-section differential uncertainty. Analytical expressions of Rayleigh scattering based on atmospheric composition usually provide better cross-section estimates than laboratory studies, e.g., Bates (1984); Eberhard (2010); Bucholtz, (1995). Using an analytical expression to compute Rayleigh extinction cross-sections is equivalent to considering the case of a single-source component (namely, the analytical function), therefore implying full correlation between all values. Under this assumption, the Rayleigh extinction cross-section differential uncertainty propagated to ozone number density and mixing ratio can be written for Rayleigh and Raman backscatter channels:

$$u_{NO3(\Delta\sigma MS)}(k) = N_a(k) \left| \frac{u_{\sigma M-1(S)}(k) + u_{\sigma M-2(S)}(k) - u_{\sigma M-3(S)}(k) - u_{\sigma M-4(S)}(k)}{\Delta\sigma_{O_3}(k)} \right| \quad (28)$$

$$u_{qO3(\Delta\sigma MS)}(k) = \left| \frac{u_{\sigma M-1(S)}(k) + u_{\sigma M-2(S)}(k) - u_{\sigma M-3(S)}(k) - u_{\sigma M-4(S)}(k)}{\Delta\sigma_{O_3}(k)} \right| \quad (29)$$

When cross-section uncertainties due to random effects only are used and for Rayleigh backscatter channels, the Rayleigh extinction cross-section differential uncertainty  $u_{NO3(\Delta\sigma MR)}$  propagated to ozone number density and mixing ratio can be written:

$$u_{NO3(\Delta\sigma MR)}(k) = \frac{2N_a(k)}{|\Delta\sigma_{O_3}(k)|} \sqrt{u_{\sigma M-1(R)}^2(k) + u_{\sigma M-3(R)}^2(k)} \quad (30)$$

$$u_{qO3(\Delta\sigma MR)}(k) = \frac{2\sqrt{u_{\sigma M-1(R)}^2(k) + u_{\sigma M-3(R)}^2(k)}}{|\Delta\sigma_{O_3}(k)|} \quad (31)$$

For Raman backscatter channels, this uncertainty component can be written:

$$u_{NO3(\Delta\sigma MR)}(k) = \frac{N_a(k)}{|\Delta\sigma_{O_3}(k)|} \sqrt{u_{\sigma M-1(R)}^2(k) + u_{\sigma M-2(R)}^2(k) + u_{\sigma M-3(R)}^2(k) + u_{\sigma M-4(R)}^2(k)} \quad (32)$$

$$u_{qO3(\Delta\sigma MR)}(k) = \frac{\sqrt{u_{\sigma M-1(R)}^2(k) + u_{\sigma M-2(R)}^2(k) + u_{\sigma M-3(R)}^2(k) + u_{\sigma M-4(R)}^2(k)}}{|\Delta\sigma_{O_3}(k)|} \quad (33)$$

Equations (29), (31) and (33) show that for a specific DIAL pair, the lidar-retrieved mixing ratio

uncertainty is directly proportional to the relative uncertainty in the Rayleigh cross-section. For a particular value of Rayleigh cross-section relative uncertainty, the DIAL pairs with longer wavelengths (e.g., 299/316 for tropospheric systems, and the Raman pair for stratospheric systems) yield larger ozone mixing ratio uncertainties.

Information / data	Type / value / equation	Notes / description
<b>Name of effect</b>	Rayleigh extinction cross section differential	
<b>Contribution identifier</b>	4b	
<b>Measurement equation parameter(s) subject to effect</b>	$\Delta\sigma_M$	Eq. 7, 8
<b>Contribution subject to effect (final product or sub-tree intermediate product)</b>	NO <sub>3</sub> , q <sub>03</sub>	Eq. 7, 8
<b>Time correlation extent &amp; form</b>	None	
<b>Other (non-time) correlation extent &amp; form</b>	None	
<b>Uncertainty PDF shape</b>	Unknown	
<b>Uncertainty &amp; units</b>	10-0.1%	From near surface to half maximum altitude. See Figs. 7 and 8.
<b>Sensitivity coefficient</b>	1	
<b>Correlation(s) between affected parameters</b>	N/A	
<b>Element/step common for all sites/users?</b>	Yes	
<b>Traceable to ...</b>	Leblanc et al., 2016c	
<b>Validation</b>	Sullivan et al., 2015 Brinksmma et al., 2000	

### 6.6.3 Interfering gases' cross section differential (4c)

Once again, an approach similar to that used for the ozone absorption and Rayleigh cross-section differentials can be used for the absorption cross-section differential of the interfering gases. The resulting uncertainty components due to random and systematic effects and propagated to ozone number density and mixing ratio can be written for NO<sub>2</sub> and SO<sub>2</sub> ( $ig=NO_2, SO_2$ ). The particular case of absorption by O<sub>2</sub> in the Herzberg and Wulf bands (applied to case study instruments) region is presented below.

Random effects, Rayleigh backscatter case:

$$u_{NO_3(\Delta\sigma_{igR})}(k) = \frac{2N_{ig}(k)}{|\Delta\sigma_{O_3}(k)|} \sqrt{u_{\sigma_{ig-1(R)}}^2(k) + u_{\sigma_{ig-3(R)}}^2(k)} \quad (34)$$

$$u_{q_{03}(\Delta\sigma_{igR})}(k) = \frac{2q_{ig}(k)}{|\Delta\sigma_{O_3}(k)|} \sqrt{u_{\sigma_{ig-1(R)}}^2(k) + u_{\sigma_{ig-3(R)}}^2(k)} \quad (35)$$

Random effects, Raman backscatter case:

$$u_{NO_3(\Delta\sigma_{igR})}(k) = \frac{N_{ig}(k)}{|\Delta\sigma_{O_3}(k)|} \sqrt{u_{\sigma_{ig-1(R)}}^2(k) + u_{\sigma_{ig-2(R)}}^2(k) + u_{\sigma_{ig-3(R)}}^2(k) + u_{\sigma_{ig-4(R)}}^2(k)} \quad (36)$$

$$u_{qO3(\Delta\sigma_{igR})}(k) = \frac{q_{ig}(k)}{|\Delta\sigma_{O3}(k)|} \sqrt{u_{\sigma_{ig-1}(R)}^2(k) + u_{\sigma_{ig-2}(R)}^2(k) + u_{\sigma_{ig-3}(R)}^2(k) + u_{\sigma_{ig-4}(R)}^2(k)} \quad (37)$$

Systematic effects, single dataset, both Rayleigh and Raman backscatter:

$$u_{NO3(\Delta\sigma_{igS})}(k) = \frac{N_{ig}(k)}{|\Delta\sigma_{O3}(k)|} |u_{\sigma_{ig-1}(S)}(k) + u_{\sigma_{ig-2}(S)}(k) - u_{\sigma_{ig-3}(S)}(k) - u_{\sigma_{ig-4}(S)}(k)| \quad (38)$$

$$u_{qO3(\Delta\sigma_{igS})}(k) = \frac{q_{ig}(k)}{|\Delta\sigma_{O3}(k)|} |u_{\sigma_{ig-1}(S)}(k) + u_{\sigma_{ig-2}(S)}(k) - u_{\sigma_{ig-3}(S)}(k) - u_{\sigma_{ig-4}(S)}(k)| \quad (39)$$

Systematic effects, two different datasets for ON and OFF wavelengths, both Rayleigh and Raman backscatter:

$$u_{NO3(\Delta\sigma_{igS})}(k) = \frac{N_{ig}(k)}{|\Delta\sigma_{O3}(k)|} \sqrt{(u_{\sigma_{ig-1}(S)}(k) + u_{\sigma_{ig-2}(S)}(k))^2 + (u_{\sigma_{ig-3}(S)}(k) + u_{\sigma_{ig-4}(S)}(k))^2} \quad (40)$$

$$u_{qO3(\Delta\sigma_{igS})}(k) = \frac{q_{ig}(k)}{|\Delta\sigma_{O3}(k)|} \sqrt{(u_{\sigma_{ig-1}(S)}(k) + u_{\sigma_{ig-2}(S)}(k))^2 + (u_{\sigma_{ig-3}(S)}(k) + u_{\sigma_{ig-4}(S)}(k))^2} \quad (41)$$

This time the ozone mixing ratio uncertainty is proportional to the relative uncertainty in the interfering gas' cross-section and to the interfering gas' mixing ratio. DIAL pairs with longer wavelengths yield a larger ozone mixing ratio uncertainty due to the large NO<sub>2</sub> cross-section values in the UV region. In "normal" NO<sub>2</sub> background conditions, the relative impact of NO<sub>2</sub> absorption on retrieved ozone remains very small for both tropospheric and stratospheric ozone systems. The ozone mixing ratio uncertainty due to SO<sub>2</sub> cross-section uncertainty is almost negligible for stratospheric DIAL pairs (Higgins band) because of the weak SO<sub>2</sub> absorption in this region compared to that of ozone. The impact of SO<sub>2</sub> absorption on retrieved ozone is therefore negligible except in the case of heavy SO<sub>2</sub> loads (i.e., 100 ppbv or above).

Information / data	Type / value / equation	Notes / description
<b>Name of effect</b>	Interfering gases' cross section differential	
<b>Contribution identifier</b>	4c	
<b>Measurement equation parameter(s) subject to effect</b>	$\Delta\sigma_{ig}$	Eq. 7, 8
<b>Contribution subject to effect (final product or sub-tree intermediate product)</b>	NO <sub>3</sub> , qO <sub>3</sub>	Eq. 7, 8
<b>Time correlation extent &amp; form</b>	None	
<b>Other (non-time) correlation extent &amp; form</b>	None	
<b>Uncertainty PDF shape</b>	N/A	
<b>Uncertainty &amp; units</b>	Variable, <10%	Depending on interfering gas species. For illustration, see Figs.7 and 8.
<b>Sensitivity coefficient</b>	1	
<b>Correlation(s) between affected parameters</b>	N/A	

<b>Element/step common for all sites/users?</b>	Yes	
<b>Traceable to ...</b>	Leblanc et al., 2016c	
<b>Validation</b>	Papayannis et al., 1990	

#### 6.6.4 Oxygen absorption cross section differential (4d)

An approach similar to that used for the other cross-section differentials can be used for the O<sub>2</sub> absorption in the region of the Herzberg and Wulf bands (Fally et al., 2000). This interfering absorption only impacts DIAL measurements using wavelengths shorter than 294 nm, i.e. the tropospheric ozone DIAL system in the case selection. In addition, the impact depends on the position of the laser line with respect to the position of the individual Herzberg lines. When the lines are coincident and the resulting absorption non-negligible, the expression of uncertainty for this component due to random and systematic effects and propagated to ozone number density and mixing ratio can be formulated in the same manner as the other interfering gases, with the exception that the O<sub>2</sub> mixing ratio  $q_{O_2}$  is a well-known constant ( $q_{O_2} \sim 0.209$ ):

- Random effects, Rayleigh backscatter case:

$$u_{NO_3(\Delta\sigma_{O_2R})}(k) = \frac{2q_{O_2}N_a(k)}{|\Delta\sigma_{O_3}(k)|} \sqrt{u_{\sigma_{O_2-1(R)}}^2(k) + u_{\sigma_{O_2-3(R)}}^2(k)} \quad (42)$$

$$u_{q_{O_3}(\Delta\sigma_{O_2R})}(k) = \frac{2q_{O_2}}{|\Delta\sigma_{O_3}(k)|} \sqrt{u_{\sigma_{O_2-1(R)}}^2(k) + u_{\sigma_{O_2-3(R)}}^2(k)} \quad (43)$$

- Random effects, Raman backscatter case:

$$u_{NO_3(\Delta\sigma_{O_2R})}(k) = \frac{q_{O_2}N_a(k)}{|\Delta\sigma_{O_3}(k)|} \sqrt{u_{\sigma_{O_2-1(R)}}^2(k) + u_{\sigma_{O_2-2(R)}}^2(k) + u_{\sigma_{O_2-3(R)}}^2(k) + u_{\sigma_{O_2-4(R)}}^2(k)} \quad (44)$$

$$u_{q_{O_3}(\Delta\sigma_{O_2R})}(k) = \frac{q_{O_2}}{|\Delta\sigma_{O_3}(k)|} \sqrt{u_{\sigma_{O_2-1(R)}}^2(k) + u_{\sigma_{O_2-2(R)}}^2(k) + u_{\sigma_{O_2-3(R)}}^2(k) + u_{\sigma_{O_2-4(R)}}^2(k)} \quad (45)$$

- Systematic effects, single dataset, both Rayleigh and Raman backscatter:

$$u_{NO_3(\Delta\sigma_{O_2S})}(k) = \frac{q_{O_2}N_a(k)}{|\Delta\sigma_{O_3}(k)|} \left| u_{\sigma_{O_2-1(S)}}(k) + u_{\sigma_{O_2-2(S)}}(k) - u_{\sigma_{O_2-3(S)}}(k) - u_{\sigma_{O_2-4(S)}}(k) \right| \quad (46)$$

$$u_{q_{O_3}(\Delta\sigma_{O_2S})}(k) = \frac{q_{O_2}}{|\Delta\sigma_{O_3}(k)|} \left| u_{\sigma_{O_2-1(S)}}(k) + u_{\sigma_{O_2-2(S)}}(k) - u_{\sigma_{O_2-3(S)}}(k) - u_{\sigma_{O_2-4(S)}}(k) \right| \quad (47)$$

- Systematic effects, two different datasets for ON and OFF wavelengths, both Rayleigh and Raman backscatter:

$$u_{NO_3(\Delta\sigma_{O_2S})}(k) = \frac{q_{O_2}N_a(k)}{|\Delta\sigma_{O_3}(k)|} \sqrt{\left( u_{\sigma_{O_2-1(S)}}(k) + u_{\sigma_{O_2-2(S)}}(k) \right)^2 + \left( u_{\sigma_{O_2-3(S)}}(k) + u_{\sigma_{O_2-4(S)}}(k) \right)^2} \quad (48)$$

$$u_{q_{O_3}(\Delta\sigma_{O_2S})}(k) = \frac{q_{O_2}}{|\Delta\sigma_{O_3}(k)|} \sqrt{\left( u_{\sigma_{O_2-1(S)}}(k) + u_{\sigma_{O_2-2(S)}}(k) \right)^2 + \left( u_{\sigma_{O_2-3(S)}}(k) + u_{\sigma_{O_2-4(S)}}(k) \right)^2} \quad (49)$$

Equations (42)-(49) show that the ozone mixing ratio uncertainty due to O<sub>2</sub> absorption is directly proportional to the relative uncertainty in the O<sub>2</sub> cross-section.

Information / data	Type / value / equation	Notes / description
<b>Name of effect</b>	Oxygen absorption cross section differential	

<b>Contribution identifier</b>	4d	
<b>Measurement equation parameter(s) subject to effect</b>	$\Delta\sigma_{ig}$	Eq. 7, 8
<b>Contribution subject to effect (final product or sub-tree intermediate product)</b>	NO <sub>3</sub> , q <sub>03</sub>	Eq. 7, 8
<b>Time correlation extent &amp; form</b>	None	
<b>Other (non-time) correlation extent &amp; form</b>	None	
<b>Uncertainty PDF shape</b>		
<b>Uncertainty &amp; units</b>	<2%	Only important for measurement wavelengths shorter than 294 nm
<b>Sensitivity coefficient</b>	1	
<b>Correlation(s) between affected parameters</b>	N/A	
<b>Element/step common for all sites/users?</b>	Yes	
<b>Traceable to ...</b>	Leblanc et al., 2016c	
<b>Validation</b>	N/A	

#### 6.6.5 Interfering gases' atmospheric profiles (4e)

Another source of uncertainty introduced in **Eq. (7)** is the *a priori* use of ancillary NO<sub>2</sub> and SO<sub>2</sub> number density or mixing ratio profiles. The term “*a priori*” here does not mean that the ozone DIAL retrieval uses a variational/optimal estimation method (it does not), but simply means that the information comes from ancillary (i.e., non-lidar) measurements or models, and is input as “truth” in the ozone DIAL processing chain. The input quantities in this case can be of a different nature, namely mixing ratio or number density (e.g., Ahmad et al., 2007; Bauer et al., 2012; Bracher et al., 2005; Brohede et al., 2007; Brühl et al., 2013; Cao et al., 2006; Hopfner et al., 2013; He et al., 2014; McLinden et al., 2014). In order to ensure self-consistency in our measurement model, input quantities independent of air number density should be chosen:

- When the input quantity independent of air number density is the interfering gas' number density  $N_{ig}$  (with uncertainty  $u_{Nig}$ ), the propagated ozone number density and mixing ratio uncertainties should be written:

$$u_{NO_3(Nig)}(k) = \left| \frac{\Delta\sigma_{ig}(k)}{\Delta\sigma_{O_3}(k)} \right| u_{Nig}(k) \quad \text{with } ig = \text{NO}_2, \text{SO}_2 \quad (50)$$

$$u_{qO_3(Nig)}(k) = \frac{1}{N_a(k)} \left| \frac{\Delta\sigma_{ig}(k)}{\Delta\sigma_{O_3}(k)} \right| u_{Nig}(k) \quad \text{with } ig = \text{NO}_2, \text{SO}_2 \quad (51)$$

- When the input quantity independent of air number density is the interfering gas' mixing ratio  $q_{ig}$  (with uncertainty  $u_{qig}$ ), the propagated ozone number density and mixing ratio uncertainties should be written:

$$u_{NO_3(qig)}(k) = N_a(k) \left| \frac{\Delta\sigma_{Nig}(k)}{\Delta\sigma_{O_3}(k)} \right| u_{qig}(k) \quad \text{with } ig = \text{NO}_2, \text{SO}_2 \quad (52)$$

$$u_{qO_3(qig)}(k) = \left| \frac{\Delta\sigma_{Nig}(k)}{\Delta\sigma_{O_3}(k)} \right| u_{qig}(k) \quad \text{with } ig = \text{NO}_2, \text{SO}_2 \quad (53)$$

Equation (53) shows that the lidar-retrieved ozone mixing ratio uncertainty due to the interfering gases is directly proportional to the gases' mixing ratio uncertainty. The NO<sub>2</sub> mixing ratio uncertainty component remains very small in most cases. One exception is for highly-polluted boundary layer conditions where NO<sub>2</sub> mixing ratio can reach 10 to 100 ppbv, resulting in ozone mixing ratio uncertainty of 0.5 to 5 ppbv for the most-commonly used DIAL wavelengths. Tropospheric ozone DIAL pairs are more affected in polluted conditions case due to the larger SO<sub>2</sub> absorption cross-section differential at the wavelengths used for tropospheric ozone DIAL.

Information / data	Type / value / equation	Notes / description
<b>Name of effect</b>	Interfering gases' atmospheric profiles	
<b>Contribution identifier</b>	4e	
<b>Measurement equation parameter(s) subject to effect</b>	$N_{ig}, q_{ig}$	Eq. 7, 8
<b>Contribution subject to effect (final product or sub-tree intermediate product)</b>	NO <sub>3</sub> , q <sub>03</sub>	Eq. 7, 8
<b>Time correlation extent &amp; form</b>	Various time scales	Will change with each measurement session due to varying experimental conditions in terms of atmospheric composition
<b>Other (non-time) correlation extent &amp; form</b>	None	
<b>Uncertainty PDF shape</b>	Poisson/normal	
<b>Uncertainty &amp; units</b>	NO <sub>2</sub> : 0.01-10% tropospheric DIAL 0.001-0.1% stratospheric DIAL SO <sub>2</sub> : 0.01-100% tropospheric DIAL 0.001-0.1% stratospheric DIAL	Uncertainty depends on wavelengths used for the measurement (tropospheric or stratospheric DIAL)
<b>Sensitivity coefficient</b>	1	
<b>Correlation(s) between affected parameters</b>	None	
<b>Element/step common for all sites/users?</b>	Yes	
<b>Traceable to ...</b>	Leblanc et al., 2016c	
<b>Validation</b>	None	

#### 6.6.6 Uncertainty owing to air number density, temperature and pressure profiles (4f)

The last input quantity to consider in our ozone DIAL measurement model is ancillary air number density. Air density is generally not estimated directly, but rather derived from air temperature and pressure. Here we provide expressions for the propagation of this uncertainty component for both cases, i.e., when air number density is considered the input quantity, and when temperature and pressure are considered the input quantities.

##### 6.6.6.1 Estimation from air number density profile

If the air number density  $N_a$  is not derived from air temperature and pressure, then its uncertainty

$u_{Na}$  can be propagated directly to ozone number density and mixing ratio. The result however will be different whether mixing ratio or number density is used as input quantity for the interfering gases' profiles:

- If number density is used as input quantity for the interfering gases' profiles:

$$u_{NO3(Na)}(k) = \left| \frac{\Delta\sigma_M + q_{O2}\Delta\sigma_{O2}(k)}{\Delta\sigma_{O3}(k)} \right| u_{Na}(k) \quad (54)$$

$$u_{qO3(Na)}(k) = \left| q_{O3} + \frac{\Delta\sigma_M + q_{O2}\Delta\sigma_{O2}(k)}{\Delta\sigma_{O3}(k)} \right| \frac{u_{Na}(k)}{N_a(k)} \quad (55)$$

- If mixing ratio is used as input quantity for the interfering gases' profiles:

$$u_{NO3(Na)}(k) = \left| \frac{\Delta\sigma_M + \Delta\sigma_{NO2}(k)q_{NO2}(k) + \Delta\sigma_{SO2}(k)q_{SO2}(k) + q_{O2}\Delta\sigma_{O2}(k)}{\Delta\sigma_{O3}(k)} \right| u_{Na}(k) \quad (56)$$

$$u_{qO3(Na)}(k) = \left| q_{O3} + \frac{\Delta\sigma_M + \Delta\sigma_{NO2}(k)q_{NO2}(k) + \Delta\sigma_{SO2}(k)q_{SO2}(k) + q_{O2}\Delta\sigma_{O2}(k)}{\Delta\sigma_{O3}(k)} \right| \frac{u_{Na}(k)}{N_a(k)} \quad (57)$$

In **Eqs. (54)-(57)**, the effect of absorption by  $O_2$  in the Herzberg and Wulf bands region is included. This term can be neglected if the ON and OFF wavelengths are longer than 294 nm. In **Eq. (57)**, it is again assumed that the interfering gases' mixing ratio profiles are independent from the air number density profile (no covariance terms involved).

### 6.6.6.2 Estimation from air temperature and pressure profile

When using radiosonde measurements, meteorological analysis, or assimilation models, the air number density is typically derived from air temperature  $T_a$  and pressure  $p_a$  following the ideal gas law (with  $k_B$  being the Boltzmann constant):

$$N_a(k) = \frac{p_a(k)}{k_B T_a(k)} \quad (58)$$

In this case, air number density is no longer the input quantity, but air temperature and pressure are. The propagation of uncertainty due to the use of an *a priori* temperature and pressure profile now depends on the degree of correlation between pressure and temperature.

- If temperature and pressure are measured or computed independently, with uncertainty estimates  $u_{Ta}$  and  $u_{pa}$  respectively, and if number density is used as input quantity for the interfering gases, the air number density uncertainty propagated to ozone number density and mixing ratio will be:

$$u_{NO3(Na)}(k) = \left| \frac{\Delta\sigma_M + q_{O2}\Delta\sigma_{O2}(k)}{\Delta\sigma_{O3}(k)} \right| N_a(k) \sqrt{\frac{u_{pa}^2(k)}{p_a^2(k)} + \frac{u_{Ta}^2(k)}{T_a^2(k)}} \quad (59)$$

$$u_{qO3(Na)}(k) = \left| \frac{\Delta\sigma_M + q_{O2}\Delta\sigma_{O2}(k)}{\Delta\sigma_{O3}(k)} \right| \sqrt{\frac{u_{pa}^2(k)}{p_a^2(k)} + \frac{u_{Ta}^2(k)}{T_a^2(k)}} \quad (60)$$

- If temperature and pressure are measured or computed independently, with uncertainty estimates  $u_{Ta}$  and  $u_{pa}$  respectively, and if mixing ratio is used as input quantity for the interfering gases, the air number density uncertainty propagated to ozone number density will be:

$$u_{NO3(Na)}(k) = \left| \frac{\Delta\sigma_M + q_{NO2}\Delta\sigma_{NO2}(k) + q_{SO2}\Delta\sigma_{SO2}(k) + q_{O2}\Delta\sigma_{O2}(k)}{\Delta\sigma_{O3}(k)} \right| N_a(k) \sqrt{\frac{u_{pa}^2(k)}{p_a^2(k)} + \frac{u_{Ta}^2(k)}{T_a^2(k)}} \quad (61)$$

- If temperature and pressure are known to be fully correlated, and if number density is used as input quantity for the interfering gases, the ozone number density uncertainty due to air number density will be written:

$$u_{NO_3(N_a)}(k) = \left| \frac{\Delta\sigma_M + q_{O_2}\Delta\sigma_{O_2}(k)}{\Delta\sigma_{O_3}(k)} \right| N_a(k) \left| \frac{u_{p_a}(k)}{p_a(k)} - \frac{u_{T_a}(k)}{T_a(k)} \right| \quad (62)$$

- If temperature and pressure are known to be fully correlated, and if mixing ratio is used as input quantity for the interfering gases, the ozone number density uncertainty due to air number density will be written:

$$u_{NO_3(N_a)}(k) = \left| \frac{\Delta\sigma_M + q_{NO_2}\Delta\sigma_{NO_2}(k) + q_{SO_2}\Delta\sigma_{SO_2}(k) + q_{O_2}\Delta\sigma_{O_2}(k)}{\Delta\sigma_{O_3}(k)} \right| N_a(k) \left| \frac{u_{p_a}(k)}{p_a(k)} - \frac{u_{T_a}(k)}{T_a(k)} \right| \quad (63)$$

Because the ozone and interfering gases' absorption cross-sections depend on temperature, the covariance terms of the cross-section differentials and the air number density covariance matrix are not strictly zero. However the correlation coefficients are expected to be very small and the assumption of two "independent" input quantities still holds.

The largest ozone uncertainty in the upper stratosphere is that due to pressure. DIAL pairs using longer wavelengths (e.g., 299/316 nm) are more impacted than pairs using shorter wavelengths, in particular the tropospheric ozone DIAL. Note that with current pressure-temperature measurement capabilities (typically 0.5 K and 0.1 hPa uncertainties), the lidar-retrieved ozone uncertainty due to temperature is about 10 times larger than that due to pressure uncertainty.

Information / data	Type / value / equation	Notes / description
<b>Name of effect</b>	External air number density, temperature and pressure profiles	This table corresponds to both 6.6.6.1 and 6.6.6.2
<b>Contribution identifier</b>	4f	
<b>Measurement equation parameter(s) subject to effect</b>	$N_a$	Eq. 7
<b>Contribution subject to effect (final product or sub-tree intermediate product)</b>	$NO_3, q_{O_3}$	Eq. 7, 8
<b>Time correlation extent &amp; form</b>	Various time scales	Will change with each measurement session due to varying experimental conditions in terms of atmospheric state
<b>Other (non-time) correlation extent &amp; form</b>	None	
<b>Uncertainty PDF shape</b>	Poisson/normal	
<b>Uncertainty &amp; units</b>	<1% for stratospheric ozone, <0.1% for tropospheric ozone. When using VMR, the uncertainty associated with this item can be substantial; linked to the uncertainty of the source information	
<b>Sensitivity coefficient</b>	1	
<b>Correlation(s) between affected parameters</b>	None	
<b>Element/step common for all sites/users?</b>	Yes	

<b>Traceable to ...</b>	Leblanc et al., 2016c	
<b>Validation</b>	Godin-Beekmann et al., 2003 Brinksma et al., 2000	

## 6.7 Spatiotemporal integration (5)

### 6.7.1 Propagation of uncertainty when combining two intensity ranges (5a)

Ozone DIAL instruments are most often designed with multiple signal intensity ranges in order to maximize the overall altitude range of the profile. Reduced signal intensity is achieved using neutral density filters or other optical systems attenuating the Rayleigh-backscattered signals, or using Raman backscatter channels which typically are 750 times weaker than Rayleigh backscatter channels. Until now, our ozone DIAL measurement model referred to a single intensity range. We now provide a formulation for the propagation of uncertainty when at least two intensity ranges are combined to form a single profile. Combining individual intensity ranges into a single profile can occur either during lidar signal processing or after the ozone number density is calculated individually for each intensity range. Here we present the case of combining ozone number density after it was calculated for individual intensity ranges. The case of combining the lidar signals is presented in **Leblanc et al., 2016a** and is applied in the selected cases for GaiaClim. The principles governing the propagation of uncertainty are the same in both cases.

A single profile covering the entire useful range of the instrument is typically obtained by combining the most accurate overlapping sections of the profiles retrieved from individual ranges. The thickness of the transition region typically varies from a few meters to a few kilometres, depending on the instrument and on the intensity ranges considered. Assuming that the transition region's bottom altitude is  $z(k_1)$  and its top altitude is  $z(k_2)$ , the combined ozone profile between a low range  $i_L$  and a high range  $i_H$ , is typically obtained by computing a weighted average of the ozone values retrieved for each range:

$$N_{O_3}(k) = w(k)N_{O_3}(k, i_L) + (1 - w(k))N_{O_3}(k, i_H) \quad k_1 < k < k_2 \text{ and } 0 < w(k) < 1 \quad (64)$$

$$q_{O_3}(k) = w(k)q_{O_3}(k, i_L) + (1 - w(k))q_{O_3}(k, i_H) \quad k_1 < k < k_2 \text{ and } 0 < w(k) < 1 \quad (65)$$

Using this formulation, all uncertainty components associated with atmospheric extinction corrections are propagated without change as they do not depend on the intensity range considered:

$$u_{NO_3(X)}(k) = u_{NO_3(X)}(k, i_L) = u_{NO_3(X)}(k, i_H) \text{ for all } k \quad (66)$$

$$u_{qO_3(X)}(k) = u_{qO_3(X)}(k, i_L) = u_{qO_3(X)}(k, i_H) \text{ for all } k \quad (67)$$

With  $X = \Delta\sigma O_3, \Delta\sigma M, Na, \Delta\sigma ig, Nig, \Delta\sigma O_2$  and  $ig = NO_2, SO_2$ .

Because of its random nature, ozone uncertainty due to detection noise for the combined profile is obtained by adding in quadrature (no covariance terms) the detection noise uncertainties of the individual ranges:

$$u_{NO_3(DET)}(k) = \sqrt{\left(w(k)u_{NO_3(DET)}(k, i_L)\right)^2 + \left((1 - w(k))u_{NO_3(DET)}(k, i_H)\right)^2} \quad k_1 < k < k_2 \quad (68)$$

$$u_{qO_3(DET)}(k) = \sqrt{\left(w(k)u_{qO_3(DET)}(k, i_L)\right)^2 + \left((1 - w(k))u_{qO_3(DET)}(k, i_H)\right)^2} \quad k_1 < k < k_2 \quad (69)$$

Assuming that the saturation correction and the background noise extraction have been applied consistently for all intensity ranges within the same data processing algorithm, the associated uncertainty components can be propagated to the combined profile assuming full correlation between the intensity ranges:

$$u_{NO_3(X)}(k) = \left|w(k)u_{NO_3(X)}(k, i_L) + (1 - w(k))u_{NO_3(X)}(k, i_H)\right| \quad k_1 < k < k_2 \quad (70)$$

$$u_{qO_3(X)}(k) = \left|w(k)u_{qO_3(X)}(k, i_L) + (1 - w(k))u_{qO_3(X)}(k, i_H)\right| \quad k_1 < k < k_2 \quad (71)$$

with  $X = SAT, BKG$ .

Information / data	Type / value / equation	Notes / description
<b>Name of effect</b>	Combining two intensity ranges	
<b>Contribution identifier</b>	5	
<b>Measurement equation parameter(s) subject to effect</b>	$\text{NO}_3, q_{\text{O}_3}$	Eq. 7, 8
<b>Contribution subject to effect (final product or sub-tree intermediate product)</b>	$\text{NO}_3, q_{\text{O}_3}$	Eq. 7, 8
<b>Time correlation extent &amp; form</b>	Same as underlying profile	See text
<b>Other (non-time) correlation extent &amp; form</b>	None	
<b>Uncertainty PDF shape</b>	Same as underlying profile	See text
<b>Uncertainty &amp; units</b>	Same as underlying profile	See text
<b>Sensitivity coefficient</b>	1	
<b>Correlation(s) between affected parameters</b>	Yes	1-4
<b>Element/step common for all sites/users?</b>	Yes	
<b>Traceable to ...</b>	Leblanc et al., 2016c	
<b>Validation</b>	Kuang et al., 2011	

## 7 Uncertainty summary

Having reviewed and propagated all the independent uncertainty components considered in our ozone DIAL measurement model, we can combine them into a single total uncertainty estimate:

- If number density is used as input quantity for the interfering gases, the combined standard uncertainty of retrieved ozone number density and mixing ratio can be written:

$$u_{NO_3}(k) = \sqrt{u_{NO_3(DET)}^2(k) + u_{NO_3(SAT)}^2(k) + u_{NO_3(BKG)}^2(k) + u_{NO_3(Na)}^2(k) + u_{NO_3(NNO_2)}^2(k) + u_{NO_3(NSO_2)}^2(k) + u_{NO_3(\Delta\sigma O_3R)}^2(k) + u_{NO_3(\Delta\sigma NO_2R)}^2(k) + u_{NO_3(\Delta\sigma SO_2R)}^2(k) + u_{NO_3(\Delta\sigma O_2R)}^2(k) + u_{NO_3(\Delta\sigma O_3S)}^2(k) + u_{NO_3(\Delta\sigma NO_2S)}^2(k) + u_{NO_3(\Delta\sigma SO_2S)}^2(k) + u_{NO_3(\Delta\sigma O_2S)}^2(k) + u_{NO_3(\Delta\sigma M)}^2(k)} \quad (72)$$

$$u_{qO_3}(k) = \sqrt{u_{qO_3(DET)}^2(k) + u_{qO_3(SAT)}^2(k) + u_{qO_3(BKG)}^2(k) + u_{qO_3(Na)}^2(k) + u_{qO_3(NNO_2)}^2(k) + u_{qO_3(NSO_2)}^2(k) + u_{qO_3(\Delta\sigma O_3R)}^2(k) + u_{qO_3(\Delta\sigma NO_2R)}^2(k) + u_{qO_3(\Delta\sigma SO_2R)}^2(k) + u_{qO_3(\Delta\sigma O_2R)}^2(k) + u_{qO_3(\Delta\sigma O_3S)}^2(k) + u_{qO_3(\Delta\sigma NO_2S)}^2(k) + u_{qO_3(\Delta\sigma SO_2S)}^2(k) + u_{qO_3(\Delta\sigma O_2S)}^2(k) + u_{qO_3(\Delta\sigma M)}^2(k)} \quad (73)$$

- If mixing ratio is used as input quantity for the interfering gases, the combined standard uncertainty of retrieved ozone number density and mixing ratio can be written:

$$u_{NO_3}(k) = \sqrt{u_{NO_3(DET)}^2(k) + u_{NO_3(SAT)}^2(k) + u_{NO_3(BKG)}^2(k) + u_{NO_3(Na)}^2(k) + u_{NO_3(qNO_2)}^2(k) + u_{NO_3(qSO_2)}^2(k) + u_{NO_3(\Delta\sigma O_3R)}^2(k) + u_{NO_3(\Delta\sigma NO_2R)}^2(k) + u_{NO_3(\Delta\sigma SO_2R)}^2(k) + u_{NO_3(\Delta\sigma O_2R)}^2(k) + u_{NO_3(\Delta\sigma O_3S)}^2(k) + u_{NO_3(\Delta\sigma NO_2S)}^2(k) + u_{NO_3(\Delta\sigma SO_2S)}^2(k) + u_{NO_3(\Delta\sigma O_2S)}^2(k) + u_{NO_3(\Delta\sigma M)}^2(k)} \quad (74)$$

$$u_{qO_3}(k) = \sqrt{u_{qO_3(DET)}^2(k) + u_{qO_3(SAT)}^2(k) + u_{qO_3(BKG)}^2(k) + u_{qO_3(Na)}^2(k) + u_{qO_3(qNO_2)}^2(k) + u_{qO_3(qSO_2)}^2(k) + u_{qO_3(\Delta\sigma O_3R)}^2(k) + u_{qO_3(\Delta\sigma NO_2R)}^2(k) + u_{qO_3(\Delta\sigma SO_2R)}^2(k) + u_{qO_3(\Delta\sigma O_2R)}^2(k) + u_{qO_3(\Delta\sigma O_3S)}^2(k) + u_{qO_3(\Delta\sigma NO_2S)}^2(k) + u_{qO_3(\Delta\sigma SO_2S)}^2(k) + u_{qO_3(\Delta\sigma O_2S)}^2(k) + u_{qO_3(\Delta\sigma M)}^2(k)} \quad (75)$$

Though **Eqs. (72)-(73)** are exclusive of **Eqs. (74)-(75)**, the resulting combined uncertainty is quantitatively identical in both formulations if we assume identical input quantity uncertainty values. The only difference between the two sets of equations is a re-distribution of the contribution of the components due to the ancillary number densities or mixing ratios. Because of the correlated terms, the ozone combined standard uncertainty should not be computed for individual intensity ranges and then merged into a single profile. Instead, the individual uncertainty components should first be propagated to the merged profile (**Eqs. (64)-(71)**) and then added in quadrature to obtain the combined standard uncertainty (**Eqs. (72)-(75)**).

Similarly, the total combined ozone density (or mixing ratio) uncertainty can be used to characterize a single profile, but should not be used for the combination of “dependent” profiles (for example a climatology computed from multiple profiles measured by the same instrument). Instead, uncertainty components due to systematic effects in altitude and/or time must be separated from components due to random effects. Typically, uncertainty due to detection noise will always be added in quadrature, while for other components, knowledge (type-A or type-B estimation) of the covariance matrix in the time and/or altitude dimension(s) will be needed. For this reason, it is recommended to always keep a trace of each individual component together with the combined standard uncertainty.

For stratospheric ozone lidar observations with the lidar located above the boundary layer, the ozone number density standard uncertainty results mainly from three components, namely, Rayleigh extinction cross section differential at the bottom of the profile, ozone absorption cross section differential in the middle of the profile, and detection noise at the top of the profile. For the derived ozone mixing ratio, the uncertainty component associated with the *a priori* use of ancillary air pressure is largely dependent on the uncertainty of the used source profile, which when

combining for instance a radio sounding with a reanalysis product, may introduce a large change in uncertainty at the switch between sources. For ozone number density and ozone mixing ratio uncertainty alike, the dominant source above 40-45 km is detection noise, depending on the site altitude and laser strength. For lidars located at lower altitudes, local air pollution may play a role and (interfering gases) should be considered when pollution conditions occur. An example of the magnitude and vertical distribution of the error contributions is illustrated in Fig. 7, which applies to one specific lidar, but -although with caution, may be taken as representative for similar stratospheric ozone lidars. In addition the error contributions due to variable atmospheric conditions may be location specific.

For tropospheric ozone lidar observations with the lidar located above the boundary layer, the combined ozone number density standard uncertainty results mainly from the ozone absorption cross section differential uncertainty. Below 12 km, the uncertainty owing to Rayleigh extinction cross section differential and detection noise are the other important components. Uncertainty owing to detection noise dominates in the upper part of the profile (above 22 km). For lidars located at lower altitudes inside the boundary layer, interfering gases may play a substantial role, depending on local circumstances and the time of observation. The total uncertainty will thus depend on location (altitude and air composition) and the chosen lidar setup (laser strength, wavelengths, etc.). An example of the magnitude and vertical distribution of the error contributions is illustrated in Fig. 8.

Uncertainty summary for stratospheric ozone:

Element identifier	Contribution name	Uncertainty contribution form	Typical value	Traceability level (L/M/H)	random, structured random, quasi-systematic or systematic?	Correlated to? (Use element identifier)
<b>1</b>	<b>Emission sub-system</b>	<b>N/A</b>	<b>Negligible</b>	<b>M</b>	<b>Systematic</b>	<b>None</b>
<b>2</b>	<b>Receiving sub-system</b>					
2a	Optical parameters	N/A	Negligible for well designed and maintained systems	M	Systematic	1
2b	Alignment	N/A	Negligible in most cases	M	Systematic	1
<b>3</b>	<b>Pre-processing</b>					
3a	Detection noise	Poiss/norm distribution	Large (10-100%) at top of profile, increasing with a factor 20 every 10 km above the ozone maximum where it is 0.3-5%)	H	Random	3b, 3c
3b	Saturation correction	N/A	Largest at bottom of	H	Systematic	3a, 3c

			partial profile (~1%), rapidly decreasing with altitude			
3c	Background noise	Poiss/norm distribution	1% near top of profile, negligible 12 km below	H	Random	3a, 3b
<b>4</b>	<b>External inputs</b>					
4a	Ozone absorption cross section differential	N/A	2%	H	Random and systematic	None
4b	Rayleigh extinction cross section differential	N/A	Largest in lower part of profile (<10%), below 1% above 20 km	H	Systematic	None
4c1	NO <sub>2</sub> cross section differential	N/A	Variable in space and time, often negligible	H	Systematic	None
4c2	SO <sub>2</sub> cross section differential	N/A	Variable in space and time, often negligible	H	Systematic	None
4d	O <sub>2</sub> cross section differential	N/A	0 (only affects wavelength shorter than 294 nm)	H	Systematic	None
4e	Profiles of interfering gases	N/A	Often negligible except in highly polluted areas	L	Random and Systematic	4c1, 4c2
4f	Number density, temperature and pressure	N/A	<1% for ozone in number density, large contribution in mixing ratio, depending on uncertainty of source	M	Random and Systematic	4a, 4b, 4c1, 4c2, 4d, 4e
<b>5</b>	<b>Spatiotemporal integration</b>					
5a	Combining two intensity ranges	N/A	Negligible	M	Random	None

Uncertainty summary for tropospheric ozone (lidar located above boundary layer):

Element identifier	Contribution name	Uncertainty contribution form	Typical value	Traceability level (L/M/H)	random, structured random, quasi-systematic or systematic?	Correlated to? (Use element identifier)
1	Emission sub-system		Negligible			
2	Receiving sub-system		Negligible			
2a	Optical parameters	N/A	Negligible for well designed and maintained systems	M	Systematic	1
2b	Alignment	N/A	Negligible in most cases	M	Systematic	1
3	<b>Pre-processing</b>					
3a	Detection noise	Poiss/norm distribution	Large (20%) at top of profile (25 km), lowest near bottom (1-2% at 3 km)	H	Random	3b, 3c
3b	Saturation correction	N/A	Largest near bottom of partial profile (>10%), rapidly decreases with altitude	H	Systematic	3a, 3c
3c	Background noise	Poiss/norm distribution	1% at top of partial profiles, decreasing with signal strength to <0.1%	H	Random	3a, 3b
4	<b>External inputs</b>					
4a	Ozone absorption cross section differential	N/A	4-6% depending on wavelength	H	Random and systematic	None
4b	Rayleigh extinction cross section differential	N/A	<10% at bottom of profile, decreasing with altitude	H	Systematic	None
4c1	NO <sub>2</sub> cross section differential	N/A	variable in space (NO <sub>2</sub> concentration) and time, often negligible	H	Systematic	None
4c2	SO <sub>2</sub> cross section differential	N/A	variable in space and time,	H	Systematic	None

			often negligible			
4e	O <sub>2</sub> cross section differential	N/A	Effect depends on laser beam characteristics, typically <0.3% at bottom of profile and decreasing with altitude	H	Systematic	None
4f	Profiles of interfering gases	N/A	Often negligible except in polluted areas	L	Random and Systematic	4c1, 4c2
4g	Number density, temperature and pressure	N/A	<0.1%	M	Random and Systematic	4a, 4b, 4c1, 4c2, 4d, 4e
5	<b>Spatiotemporal integration</b>		Negligible			
5a	Combining two intensity ranges	N/A	Negligible	M	Random	None

Ozone Uncertainty Budget for the JPL-Lidar at Mauna Loa (Hawaii)  
(March 13, 2009; 120-min. integration, 1-5 km variable vertical resolution)

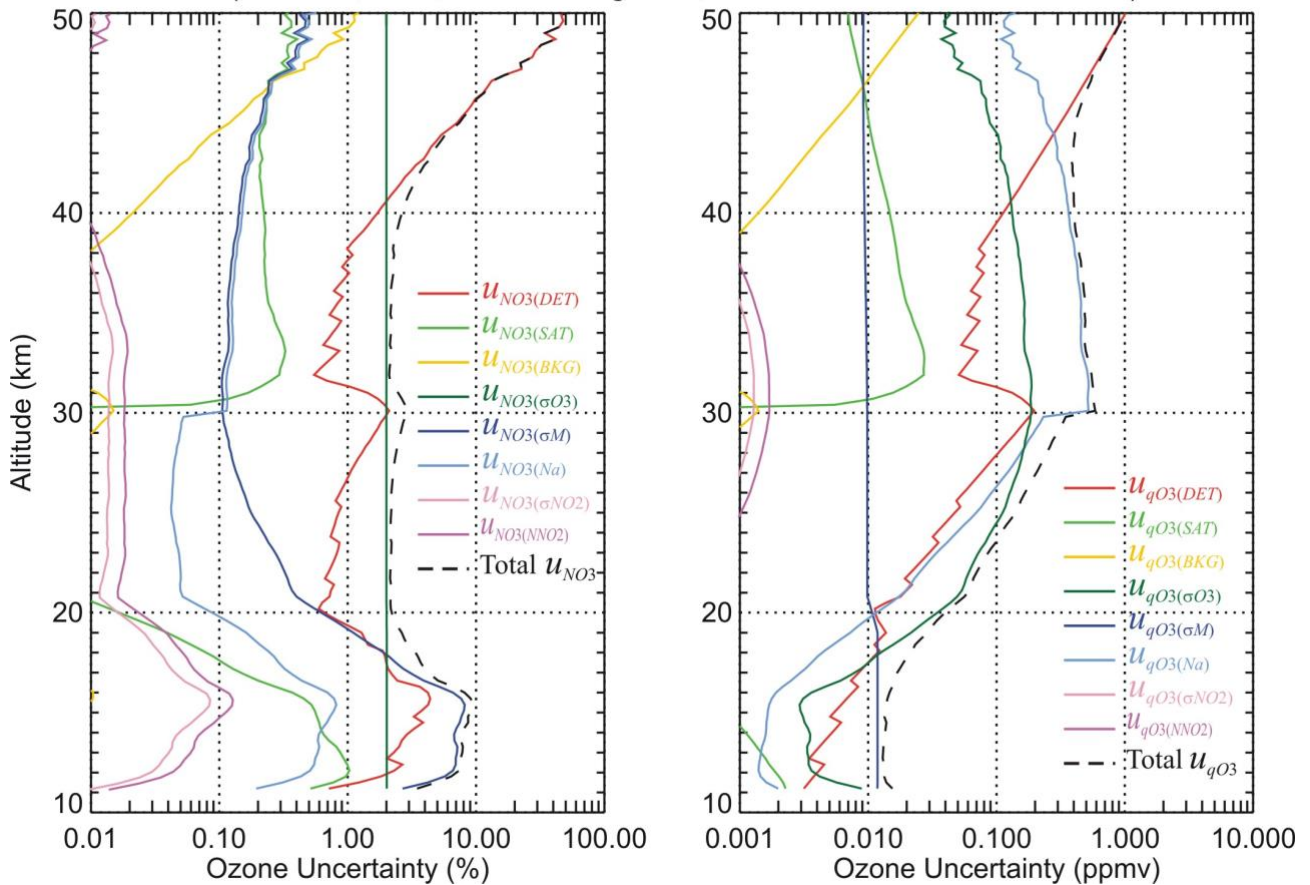


Figure 7. From Leblanc et al. (2016b, their Fig. 16). Example of ozone relative uncertainty (left) and mixing ratio uncertainty (right) budgets computed for the JPL stratospheric ozone DIAL located at Mauna Loa Observatory (Hawaii) for a nighttime observation.

Ozone Uncertainty Budget for the tropospheric ozone lidar at JPL-Table Mountain (California)  
 (November 18, 2009; 120-min. integration, 0.5-1.5 km variable vertical resolution)

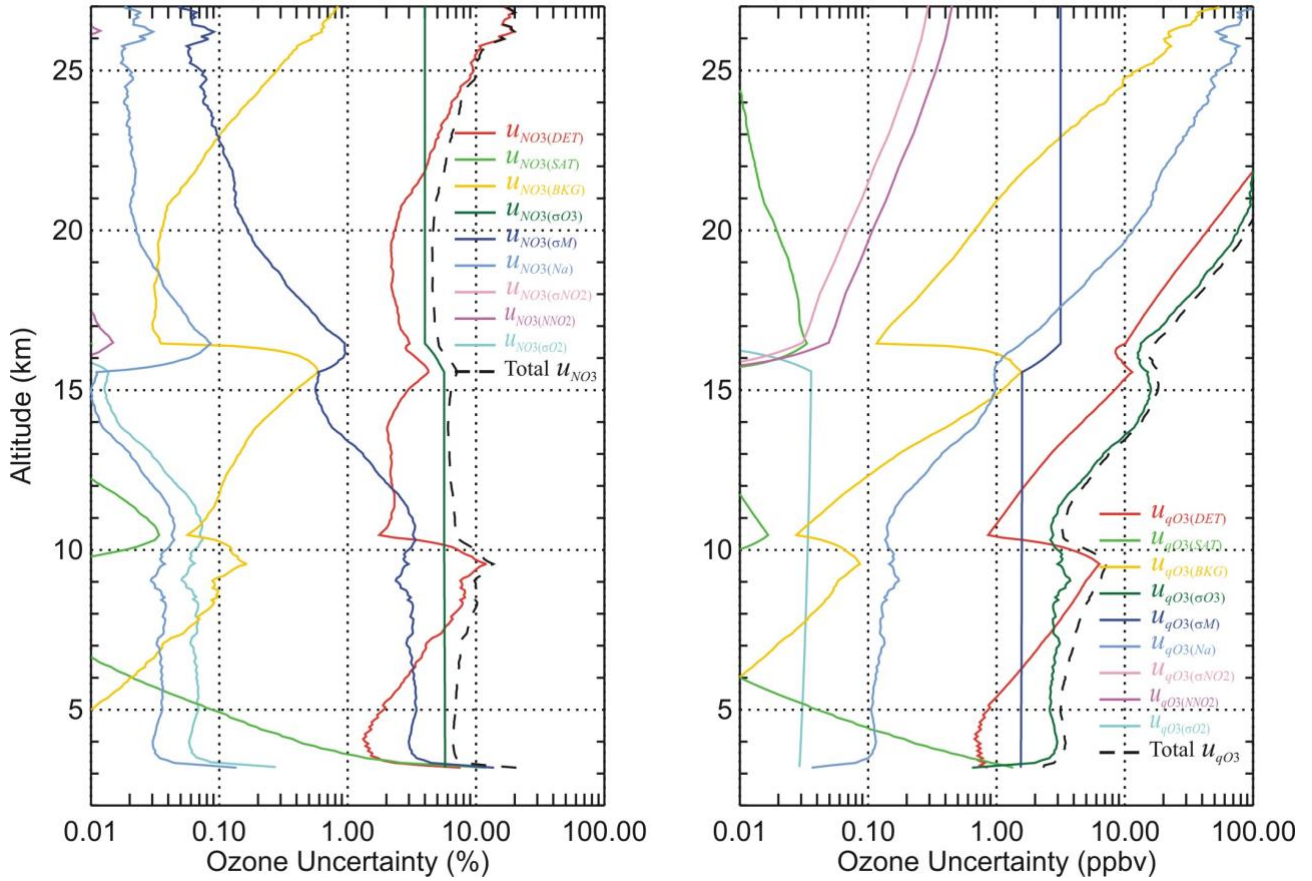


Figure 8. From Leblanc et al. (2016b, their Fig. 17). Example of ozone uncertainty budgets for the JPL tropospheric ozone lidar at Table Mountain (California) for number density (left) and mixing ratio (right) for a nighttime observation.

## 8 Traceability uncertainty analysis

Traceability level definition is given in Table 2.

Table 2. Traceability level definition table

Traceability Level	Descriptor	Multiplier
High	SI traceable or globally recognised community standard	1
Medium	Developmental community standard or peer-reviewed uncertainty assessment	3
Low	Approximate estimation	10

Analysis of the uncertainty summaries would suggest the following contributions, shown in Table 3, should be considered further to improve the overall uncertainty of the DIAL ozone profile product. The entires are given in an estimated priority order.

Table 3. Traceability level definition further action table.

Element identifier	Contribution name	Uncertainty contribution form	Typical value	Traceability level (L/M/H)	random, structured random, quasi-systematic or systematic?	Correlated to? (Use element identifier)
4f	Profiles of interfering gases	N/A	Often negligible except in polluted areas	L	Random and Systematic	4c1, 4c2
4g	Number density, temperature and pressure	N/A	<0.1%	M	Random and Systematic	4a, 4b, 4c1, 4c2, 4d, 4e

## 8.1 Recommendations

For the benefit of increasing the usability of ozone profile data originating from Differential Absorption Lidar instruments the recommendations are:

1. Application of the uncertainty propagation as outlined above and in more detailed form in Leblanc et al. (2016b, 2016c) is recommended for all ozone lidar systems, in particular those linked up in networks.
2. It should be technically feasible to set-up and operate a centralised data processing facility for ozone lidar data, which would have the obvious benefit of homogeneous data processing and therefore uncertainty budget estimation
3. Various variable uncertainty sources have been identified that are hard to quantify or highly variable in space/time or instrument-specific. These are listed as uncertainty boxes that are not filled green in Figures 8 and 9 which are expansions of those in section 5 (Figures 5 and 6). Further research into these items, and consideration of these items for individual systems when determining their PTU, is recommended.
4. In the current uncertainty analysis, use of only photon counting is assumed. It is recommended to include analysis for analog detection as well as the hybrid analog and photon counting detection modes. This may be of particular interest for the application for tropospheric ozone DIAL.

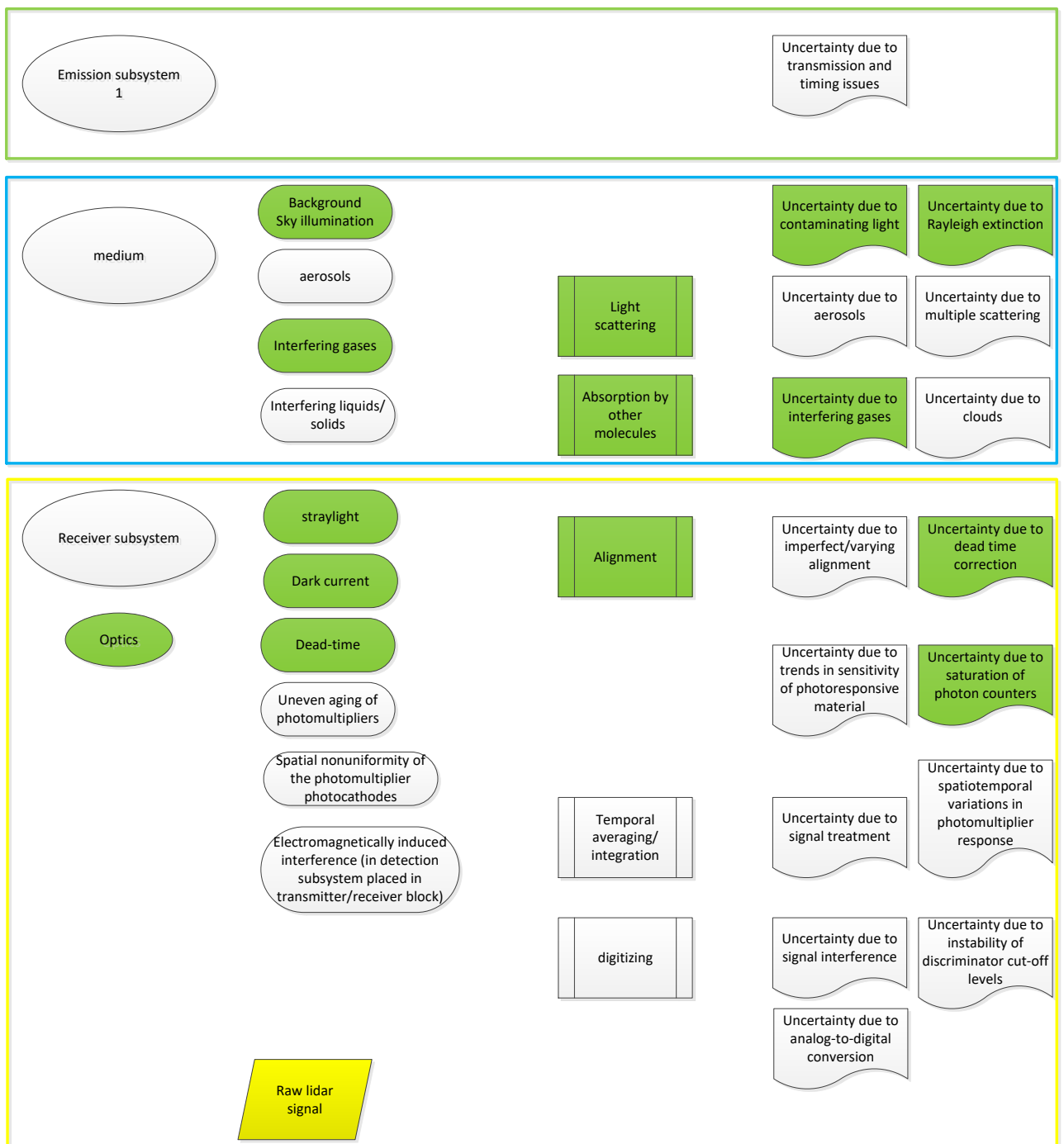


Figure 9. Expansion of flow chart in Fig. 5. Various variable uncertainty sources have been identified that are hard to quantify or highly variable in space/time or instrument-specific. These are listed as uncertainty boxes that are not filled green in the flowchart below which is an expansion of the one in section 5.

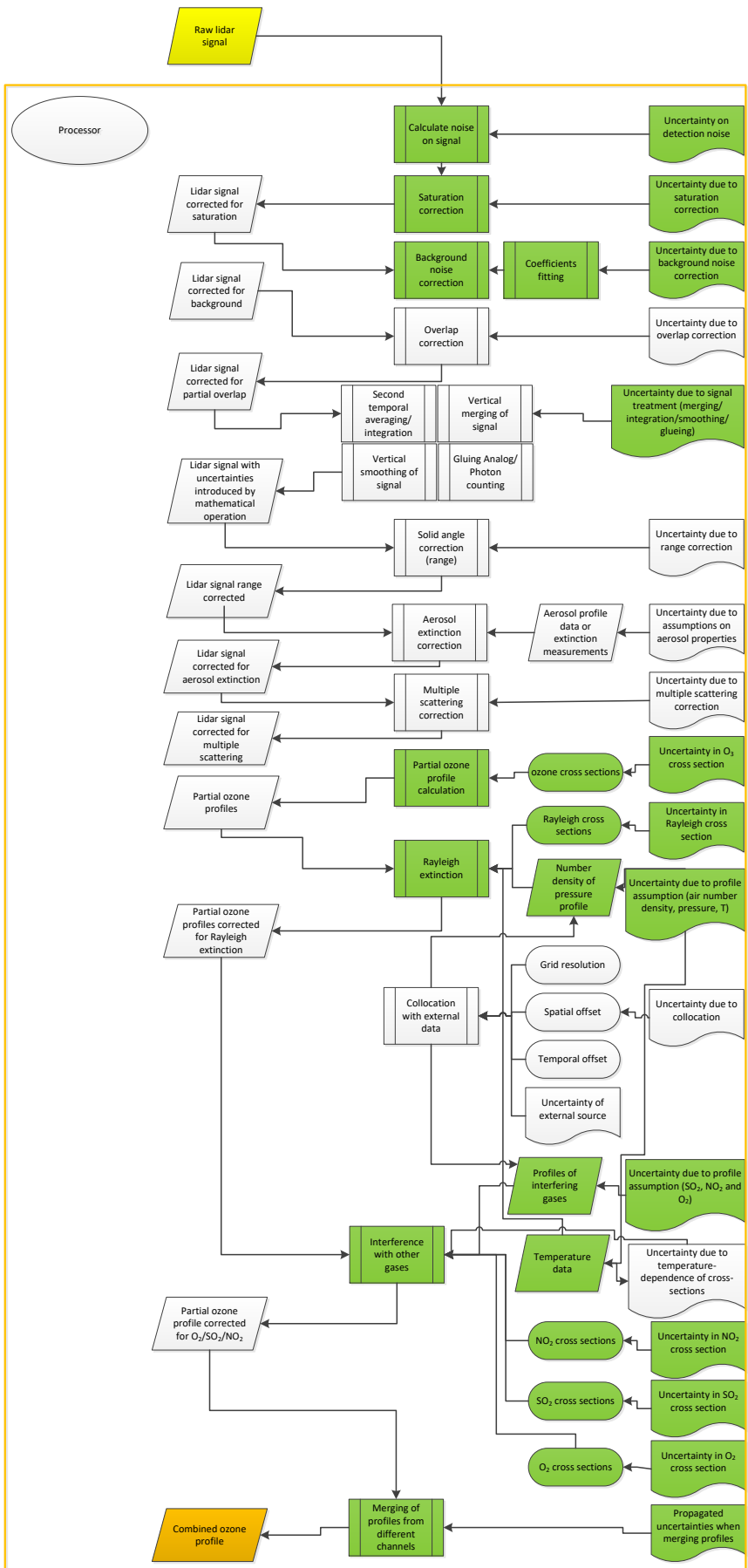


Figure 10. Expansion of flow chart in Fig. 6. Various variable uncertainty sources have been identified that are hard to quantify or highly variable in space/time or instrument-specific. These are listed as uncertainty boxes that are not filled green in the flowchart below which is an expansion of the one in section 5.

## 9 Conclusion

The ozone profile differential absorption lidar product has been assessed against the GAIA CLIM traceability and uncertainty criteria.

## References

1. Ahmad, Z., McClain, C. R., Herman, J. R., Franz, B. A., Kwiatkowska, E. J., Robinson, W. D., Bucsele, E. J., and Tzortziou, M.: Atmospheric correction for NO<sub>2</sub> absorption in retrieving water-leaving reflectances from the SeaWiFS and MODIS measurements, *Appl. Opt.*, 46(26), 6504-6512, 2007.
2. Bass, A. M., and Paur, R. J.: The Ultraviolet Cross-sections of Ozone: I. The Measurements, *Proc. Quadriennial Ozone Symp.*, Halkidiki, Greece, 606-616, 1984.
3. Bates, D. R.: Rayleigh-scattering by air, *Planet Space Sci.*, 32, 785-790, 10.1016/0032-0633(84)90102-8, 1984.
4. Bauer, R., Rozanov, A., McLinden, C. A., Gordley, L. L., Lotz, W., Russell, J. M., Walker, K. A., Zawodny, J. M., Ladstätter-Weissenmayer, A., Bovensmann, H., and Burrows, J. P.: Validation of SCIAMACHY limb NO<sub>2</sub> profiles using solar occultation measurements, *Atmos. Meas. Tech.*, 5, 1059-1084, 10.5194/amt-5-1059-2012, 2012.
5. Bogumil, K., Orphal, J., Homann, T., Voigt, S., Spietz, P., Fleischmann, O. C., Vogel, A., Hartmann, M., Kromminga, H., Bovensmann, H., Frerick, J., and Burrows, J. P.: Measurements of molecular absorption spectra with the SCIAMACHY pre-flight model: instrument characterization and reference data for atmospheric remote-sensing in the 230-2380 nm region, *J. Photochem. Photobiol. A*, 157, 167-184, 10.1016/s1010-6030(03)00062-5, 2003.
6. Bracher, A., Sinnhuber, M., Rozanov, A., and Burrows, J. P.: Using a photochemical model for the validation of NO<sub>2</sub> satellite measurements at different solar zenith angles, *Atmos. Chem. Phys.*, 5, 393-408, 10.5194/acp-5-393-2005, 2005.
7. Brinksma, E.J., Bergwerff, J.B., Bodeker, G.E., Boersma, K.F., Boyd, I.S., Connor, B.J., de Haan, J.F., Hogervorst, W., Hovenier, J.W., Parrish, A., Tsou, J.J., Zawodny, J.M., and Swart, D.P.J.: Validation of 3 years of ozone measurements over Network for the Detection of Stratospheric Change station Lauder, New Zealand, *J. Geophys. Res.*, 105(D13), 17291-17306, doi:10.1029/2000JD900143, 2000.
8. Brion, J., Chakir, A., Charbonnier, J., Daumont, D., Parisse, C., and Malicet, J.: Absorption Spectra Measurements for the Ozone Molecule in the 350-830 nm Region, *J. Atmos. Chem.*, 30, 291-299, 10.1023/a:1006036924364, 1998.
9. Bristow, M.P.: Lidar-signal compression by photomultiplier gain modulation: influence of detector nonlinearity, *Appl. Opt.* 37, 6468-6479, 1998.
10. Brohede, S., McLinden, C. A., Berthet, G., Haley, C. S., Murtagh, D., and Sioris, C. E.: A stratospheric NO<sub>2</sub> climatology from Odin/OSIRIS limb-scatter measurements, *Can. J. Phys.*, 85, 1253-1274, 10.1139/p07-141, 2007.
11. Brühl, C., Lelieveld, J., Höpfner, M., and Tost, H.: Stratospheric SO<sub>2</sub> and sulphate aerosol, model simulations and satellite observations, *Atmos. Chem. Phys. Discuss.*, 13, 11395-11425, 10.5194/acpd-13-11395-2013, 2013.
12. Burrows, J. P., Richter, A., Dehn, A., Deters, B., Himmelmann, S., and Orphal, J.: Atmospheric remote-sensing reference data from GOME - 2. Temperature-dependent absorption cross-sections of O<sub>3</sub> in the 231-794 nm range, *J. Quant. Spectr. Rad. Trans.*, 61, 509-517, 10.1016/s0022-4073(98)00037-5, 1999.
13. Bucholtz, A.: Rayleigh-scattering calculations for the terrestrial atmosphere, *Appl. Opt.*, 34(15), 2765-2773, 1995.
14. Cao, N., Fukuchi, T., Fujii, T., Collins, R. L., Li, S., Wang, Z., and Chen, Z.: Error analysis for NO<sub>2</sub> DIAL measurement in the troposphere, *Appl. Phys. B: Lasers and Optics*, 82, 141-148, 10.1007/s00340-005-2050-8, 2006.
15. Chehade, W., Gorshchev, V., Serdyuchenko, A., Burrows, J. P., and Weber, M.: Revised temperature-dependent ozone absorption cross-section spectra (Bogumil et al.) measured with the SCIAMACHY satellite spectrometer, *Atmos. Meas. Tech.*, 6, 3055-3065, doi:10.5194/amt-6-3055-2013, 2013.
16. Daumont, D., Brion, J., Charbonnier, J., and Malicet, J.: Ozone UV Spectroscopy I:

- Absorption Cross-Sections at Room Temperature, *J. Atmos Chem.*, 15, 145-155, 10.1007/bf00053756, 1992.
17. Donovan, D. P., Whiteway, J. A., and Carswell, A. I.: Correction for nonlinear photon-counting effects in lidar systems, *Appl. Opt.*, 32(33), 6742-6753, 1993.
  18. Eberhard, W. L.: Correct equations and common approximations for calculating Rayleigh scatter in pure gases and mixtures and evaluation of differences, *Appl. Opt.*, 49(7), 1116-1130, 2010.
  19. Eisele, H. and Trickl, T.: Improvements of the aerosol algorithm in ozone lidar data processing by use of evolutionary strategies, *Appl. Opt.*, 44, 2638–2651, 2005.
  20. Fally, S., Vandaele, A. C., Carleer, M., Hermans, C., Jenouvrier, A., Merienne, M. F., Coquart, B., and Colin, R.: Fourier transform spectroscopy of the O-2 Herzberg bands. III. Absorption cross-sections of the collision-induced bands and of the Herzberg continuum, *J. Mol. Spectrosc.*, 204, 10-20, 10.1006/jmsp.2000.8204, 2000.
  21. Freudenthaler, V., Linné, H., Chaikovski, A., Rabus, D., and Groß, S.: EARLINET lidar quality assurance tools, *Atmos. Meas. Tech. Discuss.*, <https://doi.org/10.5194/amt-2017-395>, in review, 2018.
  22. Godin-Beekmann, S., Porteneuve, J., and Garnier, A.: Systematic DIAL lidar monitoring of the stratospheric ozone vertical distribution at Observatoire de Haute-Provence (43.92 degrees N, 5.71 degrees E), *J. Environ. Monit.*, 5, 57-67, 10.1039/b205880d, 2003.
  23. Godin-Beekmann, S., and Nair, P. J.: Sensitivity of stratospheric ozone lidar measurements to a change in ozone absorption cross-sections, *J. Quant. Spectr. Rad. Trans.*, 113, 1317-1321, 10.1016/j.jqsrt.2012.03.002, 2012.
  24. He, H., Loughner, C. P., Stehr, J. W., Arkinson, H. L., Brent, L. C., Follette-Cook, M. B., Tzortziou, M. A., Pickering, K. E., Thompson, A. M., Martins, D. K., Diskin, G. S., Anderson, B. E., Crawford, J. H., Weinheimer, A. J., Lee, P., Hains, J. C., and Dickerson, R. R.: An elevated reservoir of air pollutants over the Mid-Atlantic States during the 2011 DISCOVER-AQ campaign: Airborne measurements and numerical simulations, *Atmos. Env.*, 85, 18-30, 10.1016/j.atmosenv.2013.11.039, 2014.
  25. Hinkley, E. D.: Laser monitoring of the atmosphere, *Topics in applied physics*, 14, Springer-Verlag, New York, 380 pp., 1976.
  26. Hopfner, M., Glatthor, N., Grabowski, U., Kellmann, S., Kiefer, M., Linden, A., Orphal, J., Stiller, G., von Clarmann, T., Funke, B., and Boone, C. D.: Sulfur dioxide (SO<sub>2</sub>) as observed by MIPAS/Envisat: temporal development and spatial distribution at 15-45 km altitude, *Atmos. Chem. Phys.*, 13, 10405-10423, 10.5194/acp-13-10405-2013, 2013.
  27. Jenouvrier, A., Merienne, M. F., Coquart, B., Carleer, M., Fally, S., Vandaele, A. C., Hermans, C., and Colin, R.: Fourier transform spectroscopy of the O-2 Herzberg bands - I. Rotational analysis, *J. Mol. Spectrosc.*, 198, 136-162, 10.1006/jmsp.1999.7950, 1999.
  28. Kuang, S., Burris, J.F., Newchurch, M.J., Johnson, S. and Long, S.: Differential absorption lidar to measure sub-hourly variation of tropospheric ozone profiles, *IEEE Trans. on GeoSc. and Rem. Sens.*, 49(1), 557-571, 2011.
  29. Leblanc, T., Sica, R. J., van Gijssel, J. A. E., Godin-Beekmann, S., Haefele, A., Trickl, T., Payen, G., and Gabarrot, F.: Proposed standardized definitions for vertical resolution and uncertainty in the NDACC lidar ozone and temperature algorithms – Part 1: Vertical resolution, *Atmos. Meas. Tech.*, 9, 4029-4049, <https://doi.org/10.5194/amt-9-4029-2016>, 2016a.
  30. Leblanc, T., Sica, R. J., van Gijssel, J. A. E., Godin-Beekmann, S., Haefele, A., Trickl, T., Payen, G., and Liberti, G.: Proposed standardized definitions for vertical resolution and uncertainty in the NDACC lidar ozone and temperature algorithms – Part 2: Ozone DIAL uncertainty budget, *Atmos. Meas. Tech.*, 9, 4051-4078, <https://doi.org/10.5194/amt-9-4051-2016>, 2016b.
  31. Leblanc, T., Sica R., van Gijssel, A., Godin-Beekmann, S., Haefele, A., Trickl, T., Payen, G., and Liberti, G.: Standardized definition and reporting of vertical resolution and uncertainty

- in the NDACC lidar ozone and temperature algorithms, ISSI Team on NDACC Lidar Algorithms Report, available for download at:  
[http://www.issibern.ch/teams/ndacc/ISSI\\_Team\\_Report.htm](http://www.issibern.ch/teams/ndacc/ISSI_Team_Report.htm), 2016c.
32. McDermid, I. S., Godin, S. M., and Lindquist L. O.: Ground-based laser DIAL system for long-term measurements of stratospheric ozone, *Appl. Opt.*, 29, 3603–3612, 1990.
  33. McDermid, I. S., Beyerle, G., Haner, D. A., and Leblanc, T.: Redesign and improved performance of the tropospheric ozone lidar at the Jet Propulsion Laboratory Table Mountain Facility, *Appl. Opt.*, 41, 7550–7555, 2002.
  34. McGee, T. J., Gross, M. R., Singh, U. N., Butler, J. J., and Kimvilakani, P. E.: Improved stratospheric ozone lidar, *Opt. Eng.*, 34, 1421–1430, 1995.
  35. McLinden, C. A., Fioletov, V., Boersma, K. F., Kharol, S. K., Krotkov, N., Lamsal, L., Makar, P. A., Martin, R. V., Veefkind, J. P., and Yang, K.: Improved satellite retrievals of NO<sub>2</sub> and SO<sub>2</sub> over the Canadian oil sands and comparisons with surface measurements, *Atmos. Chem. Phys.*, 14, 3637–3656, 10.5194/acp-14-3637-2014, 2014.
  36. Measures, R. M.: *Laser remote sensing: fundamentals and applications*, Wiley, 510 pp., 1984.
  37. Mégie, G., Allain, J. Y., Chanin, M. L., and Blamont, J. E.: Vertical Profile of Stratospheric Ozone by Lidar Sounding from Ground, *Nature*, 270, 32-9-331, 1977.
  38. Merienne, M. F., Jenouvrier, A., Coquart, B., Carleer, M., Fally, S., Colin, R., Vandaele, A. C., and Hermans, C.: Improved data set for the Herzberg band systems of O-16(2), *J. Mol. Spectrosc.*, 207, 120-120, 10.1006/jmsp.2001.8314, 2001.
  39. Mohr, P. J., Taylor, B. N., and Newell, D. B.: CODATA recommended values of the fundamental physical constants: 2006, *Rev. Mod. Phys.*, 80, 633-730, 10.1103/RevModPhys.80.633, 2008.
  40. Müller, J. W.: Dead-time problems, *Nucl. Instr. and Meth.*, 112, 47-57, 10.1016/0029-554x(73)90773-8, 1973.
  41. Papayannis, A., Ancellet, G., Pelon, J., and Megie, G.: Multiwavelength lidar for ozone measurements in the troposphere and the lower stratosphere, *Appl. Opt.*, 29, 467-476, 1990.
  42. Press, W. H.; Flannery, B. P., Teukolsky, S. A., and Vetterling W. T.: *Numerical Recipes: The Art of Scientific Computing (1<sup>st</sup> ed.)*, New York, Cambridge University Press. ISBN 978-0-521-88068-8, 1986.
  43. Serdyuchenko, A., Gorshelev, V., Weber, M., Chehade, W., and Burrows, J. P.: High spectral resolution ozone absorption cross-sections - Part 2: Temperature dependence, *Atmos. Meas. Tech.*, 7, 625-636, 10.5194/amt-7-625-2014, 2014.
  44. Simeonov, V., Larcheveque, G., Quaglia, P., van den Bergh, H. and Calpini, V.: Influence of the photomultiplier tube spatial uniformity on lidar signals, *Appl. Opt.* 38, 5186-5190, 1999.
  45. Strutt, J. W. (Lord Rayleigh): XXXIV. On the transmission of light through an atmosphere containing small particles in suspension, and on the origin of the blue of the sky, *Philos. Mag.*, 47, 375-384, 10.1080/14786449908621276, 1899.
  46. Sullivan, J. T., McGee, T. J., Leblanc, T., Sumnicht, G. K., and Twigg, L. W.: Optimization of the GSFC TROPOZ DIAL retrieval using synthetic lidar returns and ozonesondes – Part 1: Algorithm validation, *Atmos. Meas. Tech.*, 8, 4133-4143, 10.5194/amt-8-4133-2015, 2015.
  47. Weitkamp, C.: *Lidar: Range-Resolved Optical Remote Sensing of the Atmosphere*, Springer Series in Optical Sciences, 102, Springer, 460 pp., 2005.